

# Chapter III

## Effect of 3 MeV Proton Irradiation on Polymer Composites

---

### *Abstract*

*Effect of 3 MeV Proton beam on Ferric oxalate, Pd(acac), Ni-DMG and Ni powder dispersed PMMA films was studied at different ion fluences. The results obtained from various characterization techniques show the enslavement of different properties of composites upon ion beam irradiation and filler concentration. It was observed that AC electrical properties and microhardness enhanced after irradiation. Structural properties were studied by means of X-ray diffraction. FTIR analysis reveals that the ion irradiation has lead significant modifications in the chemical structure of the polymer at higher fluences and higher filler concentration. Surface morphology of the pristine and irradiated films was studied by means of AFM and SEM. The results of all characterization techniques have been correlated to give a better and apparent view of dielectric, structural, mechanical, chemical, thermal properties and surface morphology.*

### 3.0 Introduction

Polymer composites prepared by incorporating active inclusions (such as metal powder, carbon black, graphite and conducting fibers) with passive polymer matrix are incredibly demanding material in present scenario for various applications. Ion beam irradiation is also a deciding feature to achieve desire material properties.

Various types of radiation interact with matter in different ways; the primary process is the production of ions and electrically excited states of molecules which, in turn, may lead to the formation of free radicals, unsaturation etc. The mechanism of the interaction between protons and macromolecules is rather complicated. Many processes, such as the production of primary and secondary radicals, escort the formation of double bonds and transformation of C-C bonds, and autoxidation occurs in the presence of oxygen. These reactions depend on the proton beam fluence and environmental conditions during and after the irradiation. This chapter deals with the dependence of various properties of polymer composites on filler concentration and fluence of proton beam. The effect of 3 MeV proton beam irradiation on following composites have been investigated in this chapter.

- (i) PMMA+Ferric oxalate [1,2]
- (ii) PMMA+Pd(acac) [3]
- (iii) PMMA+Ni powder [4]
- (iv) PMMA+Ni-DMG [5]

PMMA was prepared by solution polymerization method as explained in section 2.2.1 of Chapter-2. Preparation method of ferric oxalate and Ni-DMG has been given in section 2.2.2. The composites were prepared by vigorous mixing of filler and polymer and films were prepared by casting method as discussed in section 2.2.3. These films were irradiated with 3 MeV proton beam at Cyclotron centre,

Punjab University, Chandigarh, India at the fluences of  $5 \times 10^{12}$  and  $1 \times 10^{13}$  ions/cm<sup>2</sup>. AC electrical, mechanical, structural, chemical properties and surface morphology have been studied for pristine and irradiated samples.

### **3.1 Effect of proton beam on PMMA+Fo composites**

#### **3.1.1 AC electrical properties**

##### *(i) AC electrical Conductivity*

The a.c. conductivity of the composites as a function of the frequency, fluence, and filler concentration has been studied and shown in Fig. 3.1(a-d). AC conductivity was calculated using eq. 2.3.13 as discussed in Chapter 2. Fig. 3.1 shows that conductivity at low frequency (up to  $10^4$  Hz) looks like a straight line for all the composites, typical of hopping conduction [6]. It is known that electrical conductivity of such composites depends on the type and concentration of the dispersed compound. The increase in conductivity is related to a possible increase in the number of conduction paths created between the filler particles aggregate in the composite in addition to a decrease in the width of potential barriers within the bulk regions of high conductivity. Therefore, more charge carriers may be able to “hop” by tunnelling; resulting in the increase in the bulk conductivity and it also increases with increasing filler concentration [7-9]. Generally, enhancement in a.c. electrical conductivity by increasing filler contents is attributed to the electronic interaction processes taking place in the composites.

At low filler concentration, the transport charge carriers are very low hence conduction is only due to hopping and tunnelling through a non-conducting medium between the neighbouring particles. Therefore, the overall conductivity of such a composite is low.

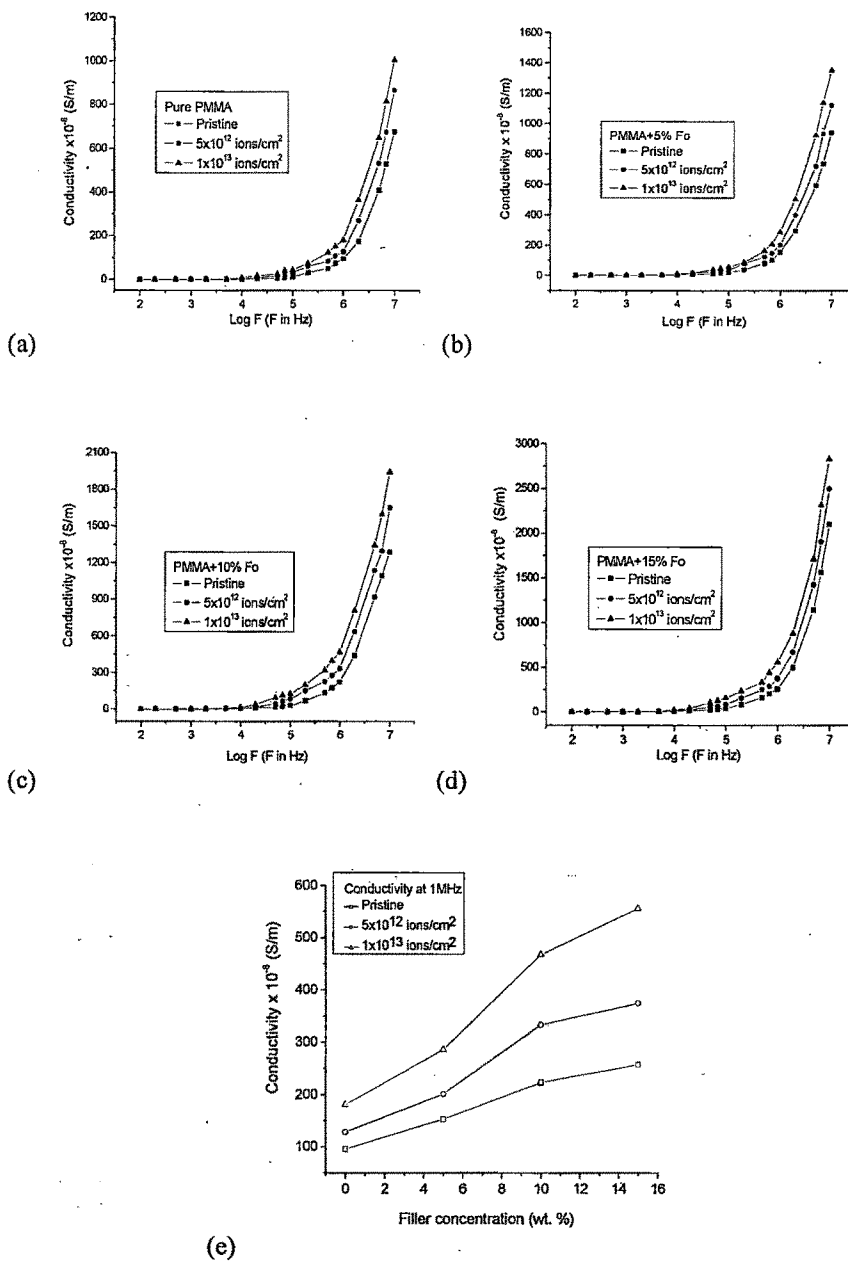


**Fig.3.1** Conductivity versus log frequency for pristine and irradiated films of (a) Pure PMMA, (b) PMMA+5% Fo, (c) PMMA+10% Fo, (d) PMMA+15% Fo (e) Conductivity vs. filler concentration at 1 MHz.

As concentration of the filler increases, the gap between the particles diminishes and conductivity slowly increases because charge transport becomes easier [10]. From Fig. 3.1(e) it was observed that the conductivity is enhanced with the increase in concentration of filler. Conductivity is further observed to increase upon irradiation. Irradiation is expected to promote the metal to polymer bonding and convert polymeric structure into a hydrogen-depleted carbon network. It is this carbon network that is believed to make the polymer more conductive [11, 12].

*(ii) Dielectric properties*

Dielectric constant was calculated using the formula 2.3.15 (section 2.3.1) of Chapter-2. It is observed that the relative dielectric permittivity is almost constant in the wide frequency range up to 100 kHz as shown in Fig. 3.2(a-d). This is because of the constant motion of free charge carriers at these frequencies. As the frequency increases further, the charge carriers migrate through the dielectric and get trapped against a defect sites. They induce an opposite charge in its vicinity, as a result the motion of charge carriers is slowed down and the value of dielectric constant decreases. The decrease in dielectric constant at higher frequency can be explained by Jonscher's power law i.e.  $\epsilon \propto \omega^{-n}$  where  $0 < n < 1$  [13].

Due to doping, the quantity of the accumulated charge increases because of the polarization of the polymer/metal at interfaces. The polarization makes an additional contribution to the charge quantity. From this point of view, the dielectric constant of the composites will be higher than the pure polymer [14]. Our experimental results also support this explanation as seen in Fig. 3.2(e). It is observed that the value of  $n$  increases from 0.65 to 0.98 with ion fluence for pure PMMA. Similar results are also obtained for doped PMMA after irradiation. This

may be due to the dominance of metal to polymer bonding due to irradiation, which reduces the dipole polarization and as a result slop (n) increases [15].

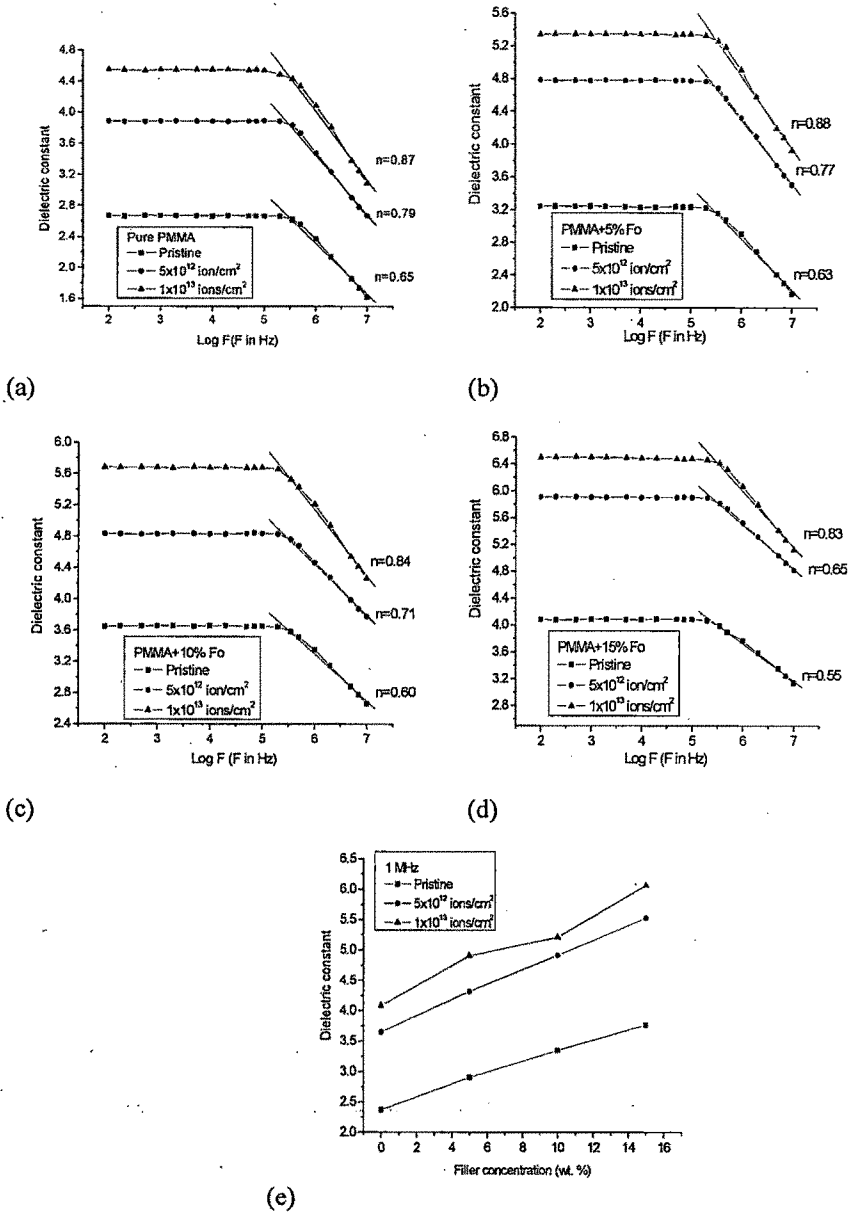
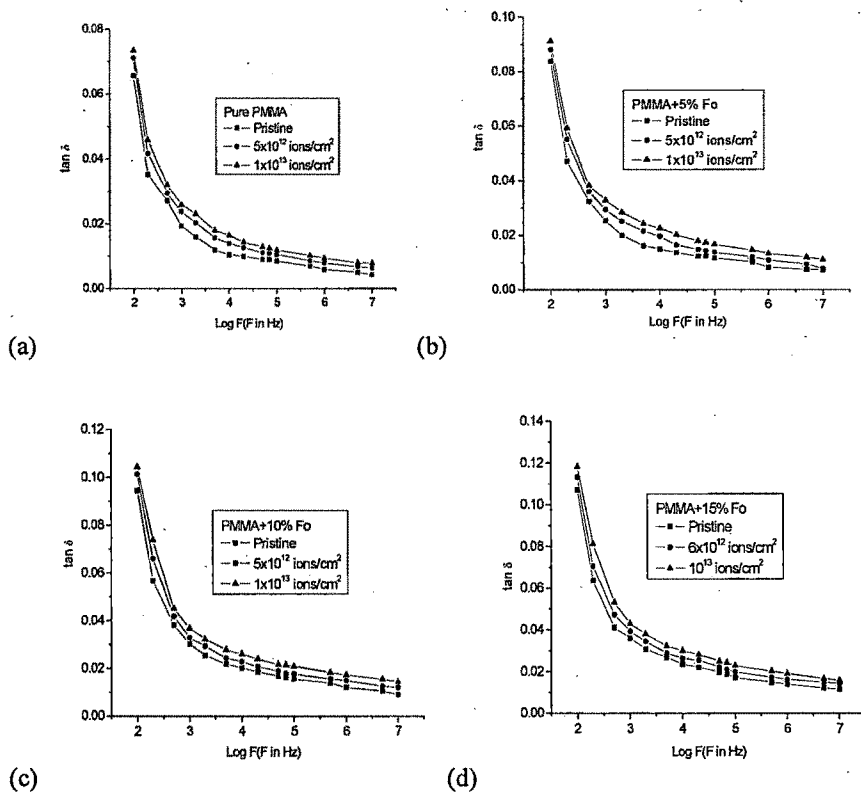


Fig. 3.2 Dielectric constant vs log frequency for Pristine and irradiated films of (a) Pure PMMA. (b) PMMA+5%Fo. (c) PMMA+10%Fo. (d) PMMA+15%Fo (e) Dielectric constant vs. filler concentration at 1 MHz

The dielectric loss is the power dissipated in a dielectric as heat when the dielectric is exposed to an electric field. Dielectric loss tangent ( $\tan\delta$ ) is defined as a ratio of energy lost or dissipated per cycle to the energy stored. It was measured directly using LCR meter/Impedance gain phase analyzer. Fig 3.3(a-d) represents the dielectric loss versus log frequency for pristine and irradiated samples.



**Fig. 3.3 Dielectric loss ( $\tan\delta$ ) vs log frequency for pristine and irradiated films of (a) Pure PMMA (b) PMMA+5%Fo (c) PMMA+10%Fo (d) PMMA+15%Fo.**

It is observed that the dielectric loss decreases exponentially with increasing the frequency and then became less dependent at higher frequency. It is also observed that loss factor increases with Fo concentration and also with the ion fluence. The growth in  $\tan\delta$  and thus increase in conductivity is brought about by an increase in the conduction of residual current and absorption current [13].

### 3.1.2 Microhardness

The Vicker's microhardness of all the samples was calculated using equation 2.3.16 (Section 2.3.2) of Chapter 2. Fig. 3.4(a-d) shows Vicker's microhardness versus applied load for pristine and irradiated composite films. The hardness is known to be influenced by surface effects. Particularly at low penetration depths, the strain hardening modifies the true hardness of the material.

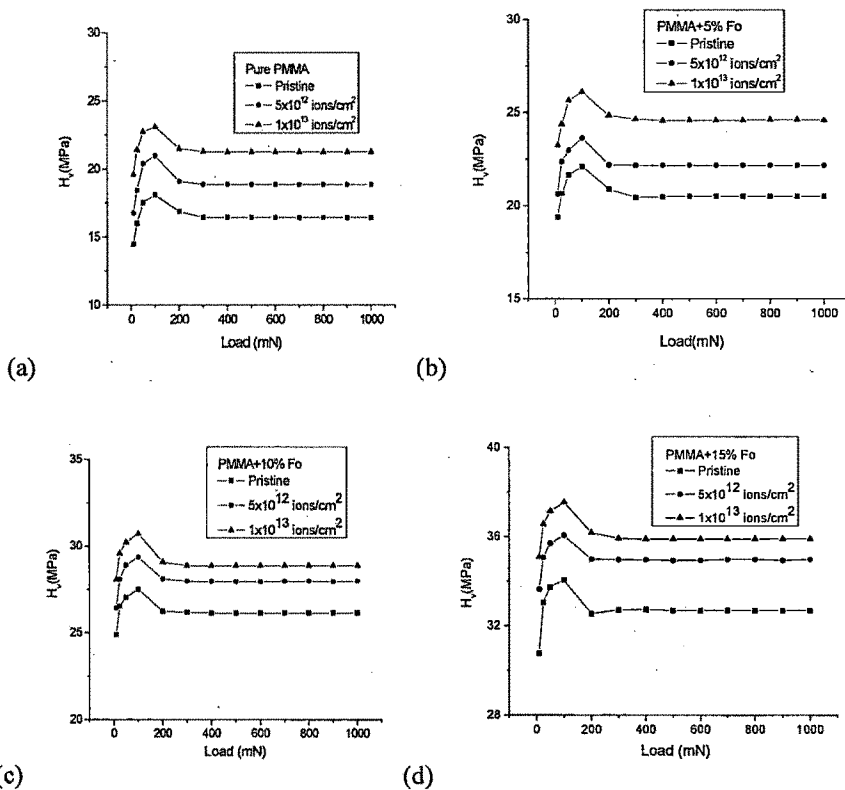


Fig. 3.4 Microhardness vs applied load for pristine and irradiated films of (a) Pure PMMA (b) PMMA+5%Fo (c) PMMA+10%Fo (d) PMMA+15%Fo.

The microhardness indentations were carried out on the surface of the pristine and irradiated films at room temperature under different applied loads from 10–1000 mN and at a constant loading time of 30s. It has been observed that microhardness

(Hv) value increases with the load up to 100 mN and then decreases and become saturated beyond the load of 300 mN. At higher loads, beyond 300 mN, the interior of the bulk specimen is devoid of surface effects. Hence, the hardness value at higher loads represents the true value of the bulk and it is consequently independent of the load. It is found that hardness increases for ferric oxalate dispersed PMMA films. It may be due to the improvement in bonding properties [16]. The hardness also increases upon irradiation. This may be attributed to hydrogen depleted carbon network, which further enhance hardness [17, 18].

### 3.1.3 Atomic force microscopy

Surface morphology of pristine and irradiated composites was studied using atomic force microscopy in contact mode with silicon nitride ( $\text{Si}_3\text{N}_4$ ) tip. The 3-dimension morphology of pristine and irradiated (at a fluence of  $5 \times 10^{12}$  ions/ $\text{cm}^2$ ) samples are shown in Fig. 3.5 (a-h) in  $2 \times 2 \mu\text{m}^2$  area. Average surface roughness was observed to decrease from 8.6 to 6.3 nm for Pure PMMA after irradiation and surface becomes relatively smoother. Similarly, it decreases from 27.8, 29.6 and 46.4 nm to 25.6, 22.0 and 32.5 nm respectively for 5, 10 and 15% ferric oxalate dispersed PMMA composites after irradiation. This smoothness is attributed to defect enhanced surface <sup>diffusion</sup> [19-21]. However the increase in roughness from 8.6nm (pure PMMA) to 46.4nm (PMMA+15% Fo) is due to increase in density and size of metal particle on the surface of PMMA films [22, 23].

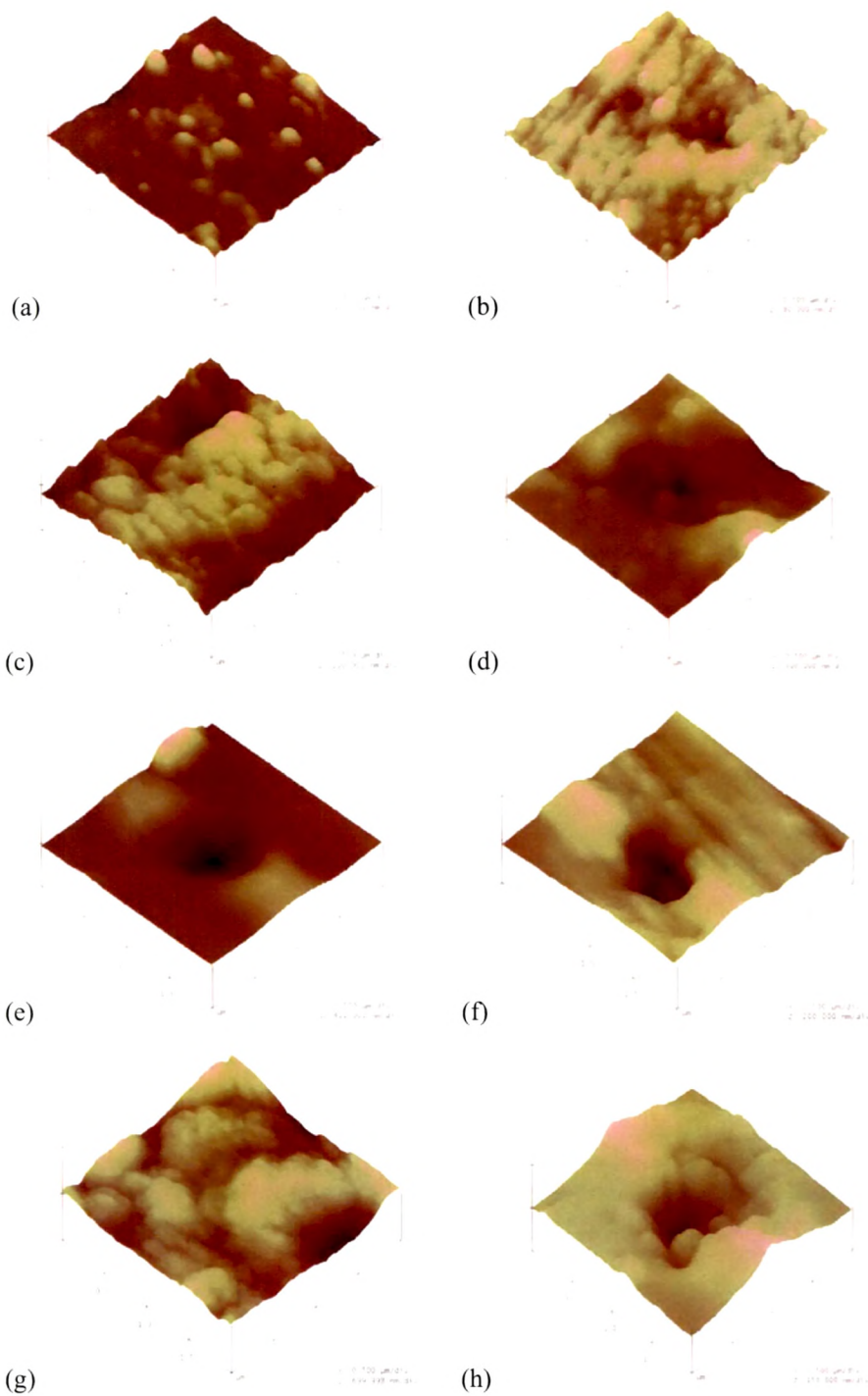


**Fig. 3.5 AFM image of (a) Pure PMMA (Pristine) (b) Pure PMMA (Irradiated) (c) PMMA+5% Fo (Pristine) (d) PMMA+5% Fo (Irradiated) (e) PMMA+10% Fo (Pristine) (f) PMMA+10% Fo (Irradiated) (g) PMMA+15% Fo (Pristine) (h) PMMA+15% Fo (Irradiated) films**

### 3.1.4 FTIR analysis

Figure 3.6 shows the FTIR spectra of pristine and irradiated samples.

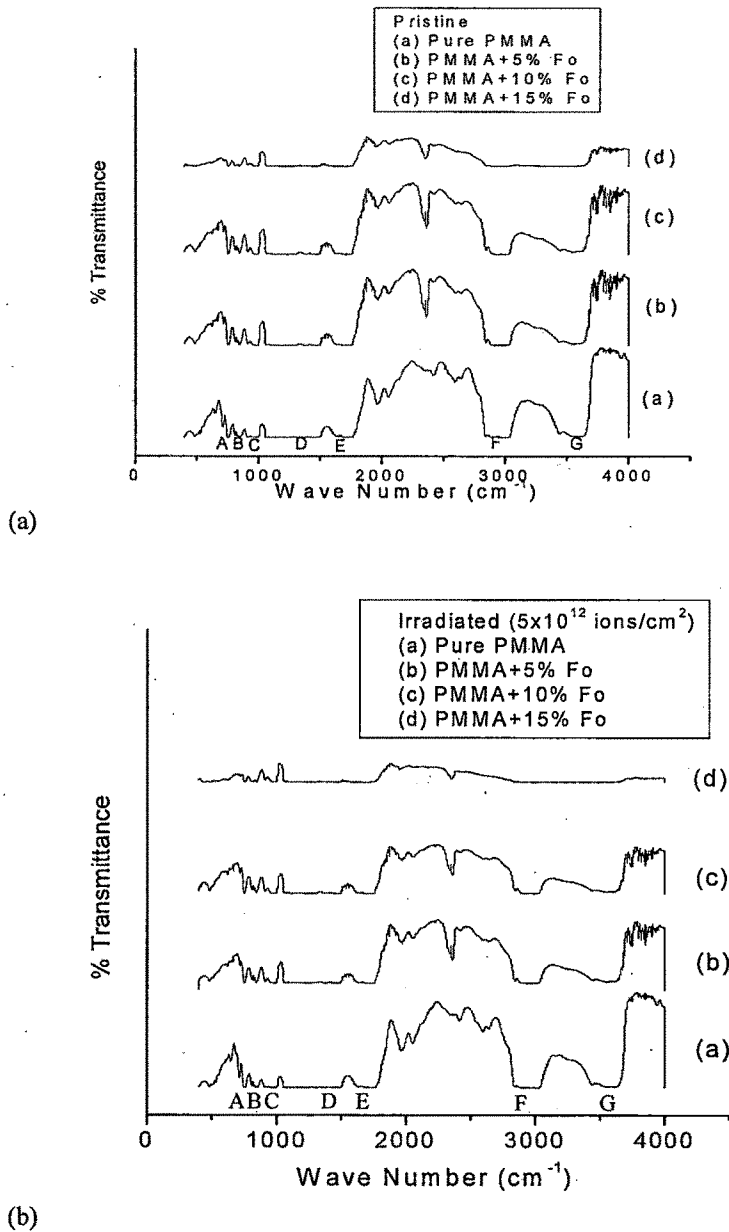


Fig. 3.6 FTIR spectra of pristine and irradiated ( $5 \times 10^{12}$  ions/cm<sup>2</sup>) PMMA composites.

The absorption bands are obtained from the pristine spectrum are identified as (A) 730  $\text{cm}^{-1}$ :  $\text{CH}_2$  (C-H rocking), (B) 816  $\text{cm}^{-1}$ :  $\text{CH}_3$  (C-H rocking), (C) 950  $\text{cm}^{-1}$ : carboxylic ester (D) 1270  $\text{cm}^{-1}$ : C-C-O stretching, (E) 1715  $\text{cm}^{-1}$ : R-C=O (kepton of ester) (F) 2820-3080  $\text{cm}^{-1}$ : C-H stretching (G) 3610  $\text{cm}^{-1}$ : OH free stretching vibration [24]. It is observed that there is no significant change in overall structure of the polymer but changes in peak intensities were observed after irradiation. The reduction in peak intensities of the irradiated sample is attributed to the breakage of the chemical bonds and formation/emission of low molecule gases and radicals due to irradiation.

### **3.1.5 Conclusion**

Proton irradiation has significantly enhanced the electrical and mechanical properties of the Fo doped PMMA composites. This is attributed to the fact that the radiation exposure on the polymer composite converts the polymeric structure in to hydrogen depleted carbon network and promotes good adhesion between metal and polymer. This makes the composite more conductive and harder. The dielectric constant/loss shows frequency dependent behavior and change significantly after irradiation. The surface morphology reveals that the surface becomes smoother after irradiation. This is attributed to the defect-enhanced surface diffusion. The FTIR spectra also reveal the breakage of bonds and scissioning of polymer chain due to ion beam irradiation.

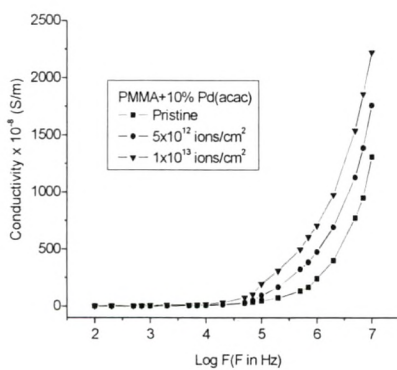


## 3.2 Effect of proton beam on PMMA+Pd(acac) composites

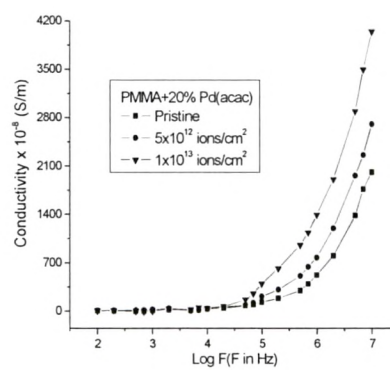
### 3.2.1 AC electrical properties

#### (i) AC electrical Conductivity

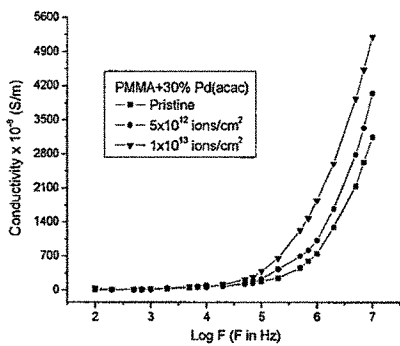
Fig. 3.7(a-d) shows the variation of conductivity with log frequency and fluence of ion beam. AC conductivity was calculated using eq. 2.3.13 (section 2.3.1) of Chapter 2. In low frequency range, the conductivity is obtained due to hopping mechanism [6]. Fig. 3.7(e) shows the dependence of conductivity on concentrations of filler. It was observed that conductivity increases with filler concentration. It is attributed to the conductive nature of Pd(acac). Electrical conductivity of such composites depends on the type and concentration of the filler. Generally, the conductivity increases on increasing the concentration of metallic compound in polymer matrix. Ion beam irradiation is expected to promote the metal to polymer adhesion and convert the polymeric structure to a hydrogen depleted carbon network. It is this carbon network that is believed to make the polymer more conductive [11, 12].



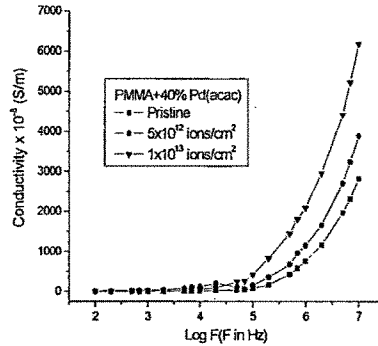
(a)



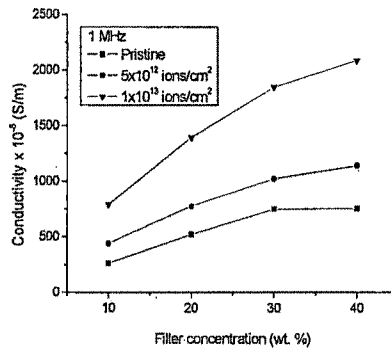
(b)



(c)



(d)



(e)

Fig. 3.7 Conductivity versus log frequency of pristine and irradiated films of (a) PMMA+10%Pd(acac) (b) PMMA+20%Pd(acac) (c) PMMA+30%Pd(acac) (d) PMMA+40%Pd(acac). (e) Conductivity vs. filler concentration at 1 MHz

### (ii) Dielectric properties

Dielectric constant was calculated using equation 2.3.15 as described in Chapter-2.

Figure 3.8(a-d) shows the variation in dielectric constant with log frequency. It remains almost constant up to 100 kHz because the motion of charge carriers is almost constant at these frequencies. Beyond this frequency, the dielectric constant decreases. The decrease in dielectric constant at higher frequency can be explained by Universal law of dielectrics given by  $\epsilon \propto f^{-n}$  where  $0 < n < 1$  [13]. Due to dispersion of organometallic compound, the quantity of the accumulated charge will increase because of the polarization at polymer/metal interfaces.

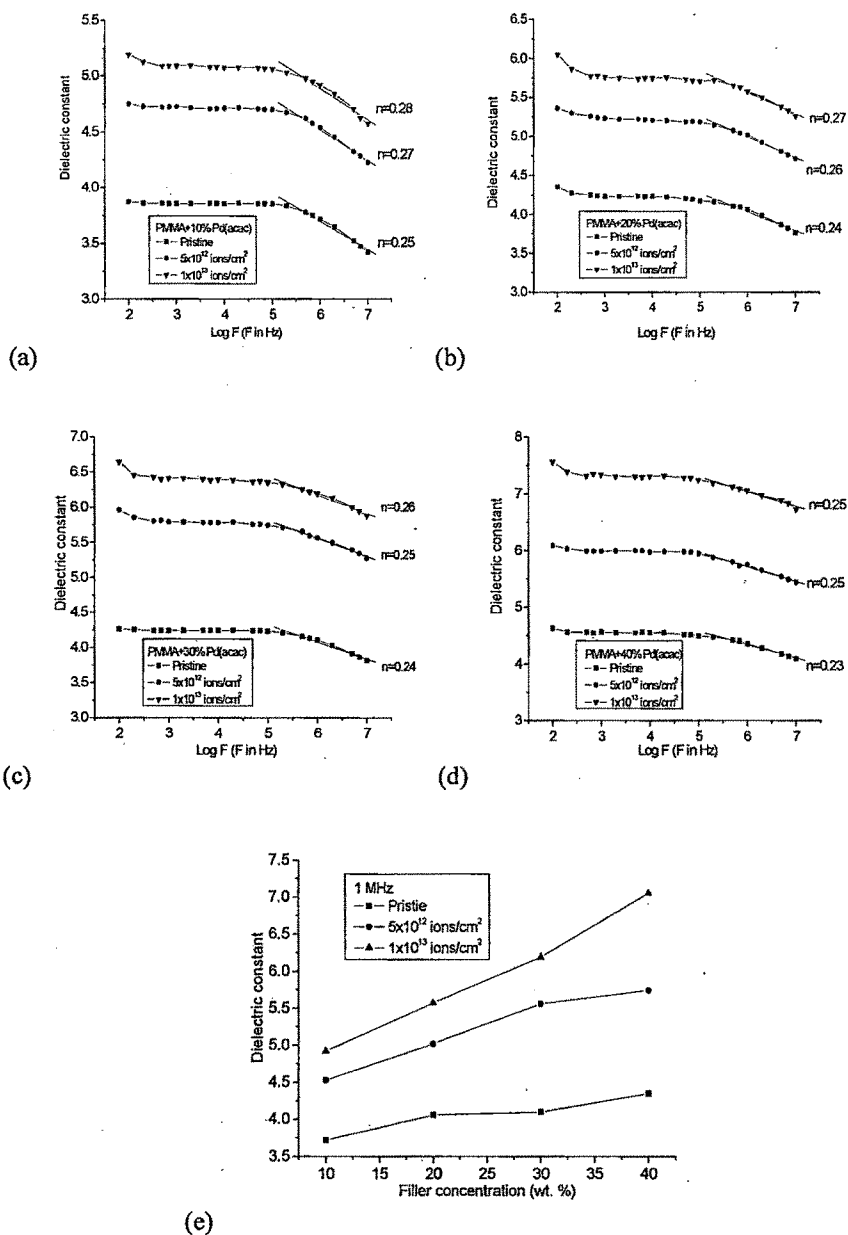
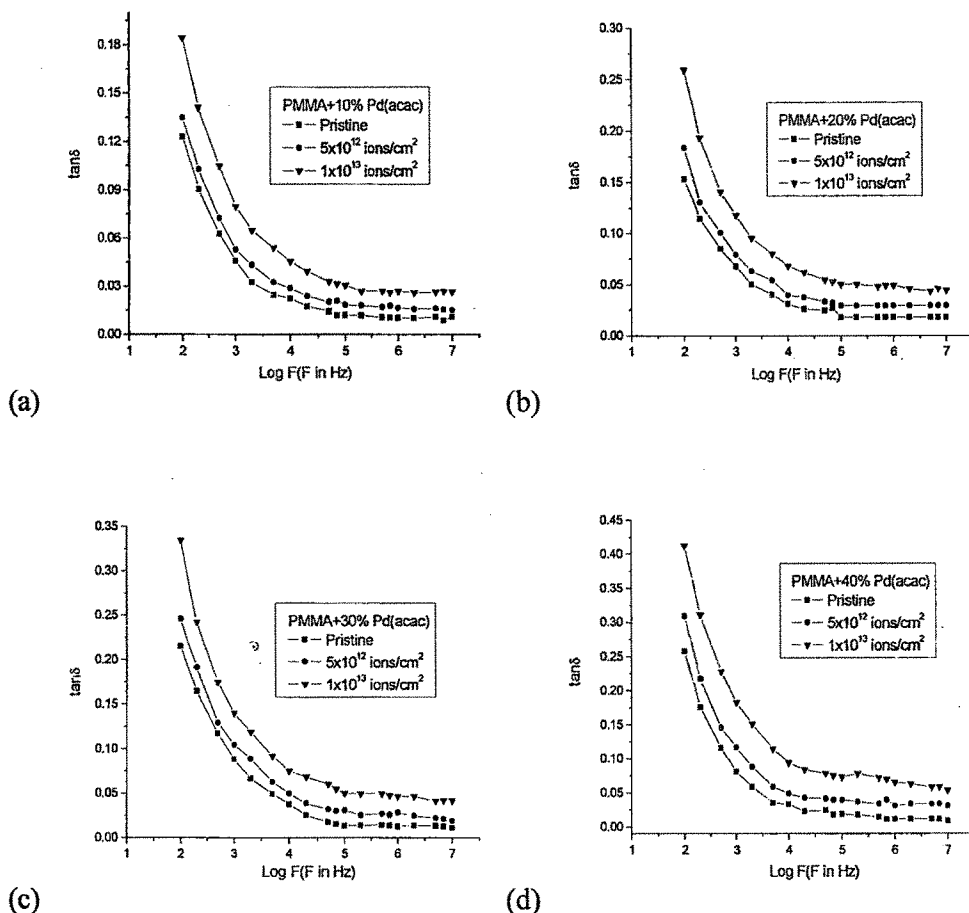


Fig. 3.8 Dielectric constant versus log frequency of pristine and irradiated films of (a) PMMA+10%Pd(acac) (b) PMMA+20%Pd(acac) (c) PMMA+30%Pd(acac) (d) PMMA+40%Pd(acac). (e) Dielectric constant vs. filler concentration at 1 MHz

The polarization makes an additional contribution to the charge quantity. Therefore the dielectric constant of the composites will increase with filler concentration [14].

Fig. 3.8 (e) shows variation in dielectric constant with filler concentration at 1 MHz. Dielectric constant also increases upon irradiation.

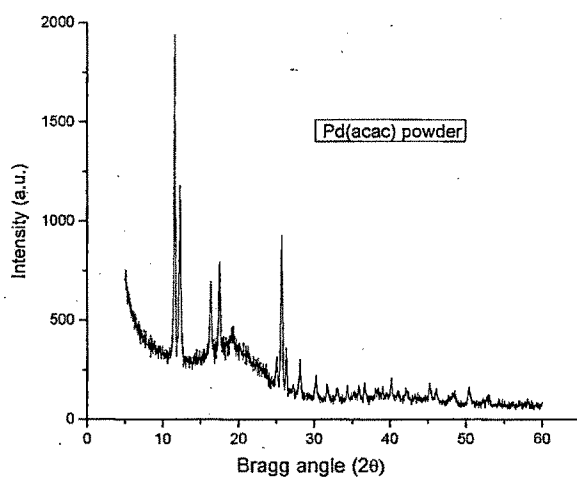


**Fig. 3.9** Dielectric loss versus log frequency of pristine and irradiated films of (a) PMMA+10%Pd(acac) (b) PMMA+20%Pd(acac) (c) PMMA+30%Pd(acac) (d) PMMA+40%Pd(acac)

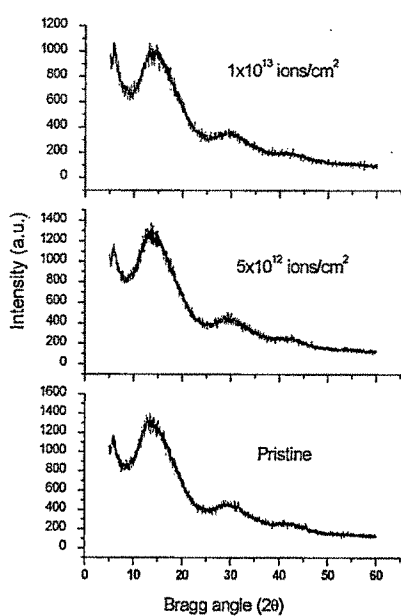
Fig. 3.9 (a-d) shows strong frequency dependence of dielectric loss. It decreases exponentially and then became less dependent on frequency. This is because the induced charges gradually fail to follow the reversing field causing a reduction in the electronic oscillations as the frequency is increased. The increase in dielectric loss with increasing filler contents may be attributed to the interfacial polarization mechanism of the heterogeneous system. It is noticed that dielectric loss further increases with fluence [24].

### 3.2.2 X-ray diffraction

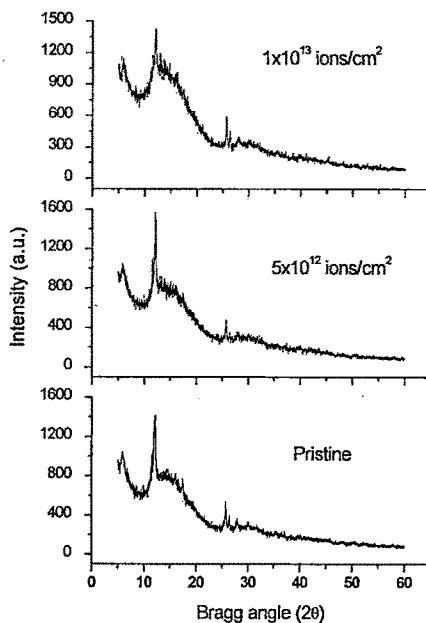
Fig.3.10 (a) shows the X-ray diffraction pattern for Pd(acac) powder. It shows crystalline behavior of the organometallic compound. The most prominent peaks obtained at  $2\theta$  are  $12.1^\circ$ ,  $17.4^\circ$ ,  $25.7^\circ$  and  $28.0^\circ$ . Identical peaks were obtained for the polymer composites because of the presence of different concentrations of Pd(acac) in PMMA. Fig. 3.10 (b-f) shows the diffraction patterns of pristine and irradiated composites with different filler concentrations. The spectrum represents the amorphous nature of the pure PMMA and semi-crystalline nature of the composites.



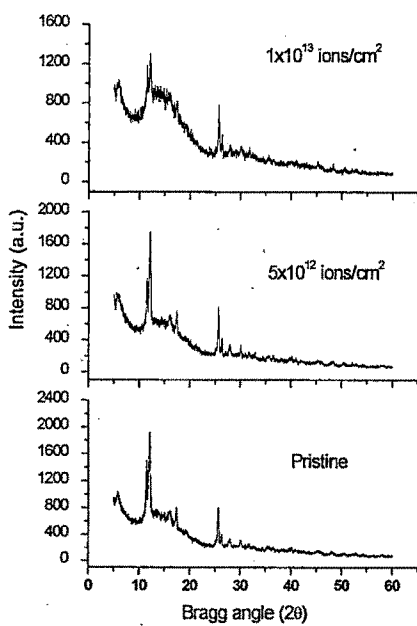
(a)



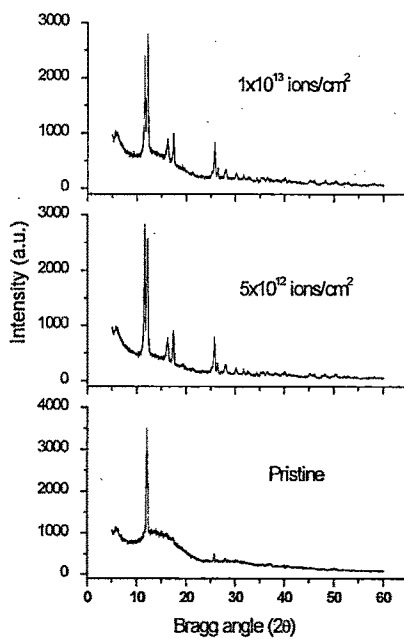
(b)



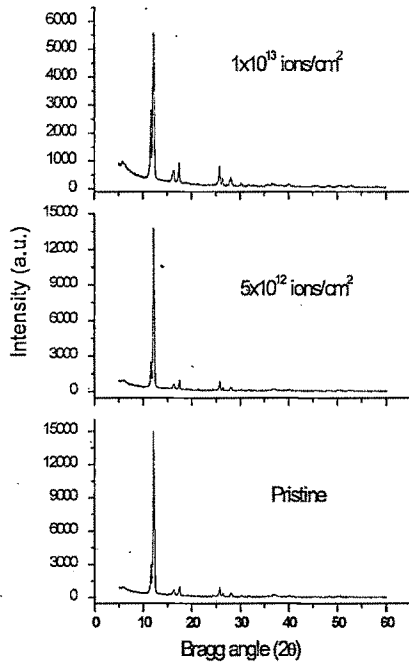
(c)



(d)



(e)



(f)

**Fig.3.10 XRD spectra of pristine and irradiated films of (a)Pd(acac) powder (b)Pure PMMA (c) PMMA+10% Pd(acac) (d)PMMA+20% Pd(acac) (e)PMMA+30%Pd(acac) (f) PMMA+40% Pd(acac)**

The crystallite size was calculated before and after the irradiation using Scherrer's formula [25] as discussed in section 2.3.3 of Chapter-2.

$$D = \frac{K\lambda}{l \cos \theta}$$

where K is constant approximately equal to unity and related to the crystalline shape,  $l$  is FWHM of the diffraction peak, D is crystalline size and  $\theta$  is the angle between the atomic plane and both the incident and reflected beams [26]. Irradiation deposited large amount of energy in the material and leads to decrease in crystallite size. This may be attributed to splitting of crystalline grains. Percentage crystallintiy of the composites was determined by area ratio method. In this method the areas of amorphous and crystalline parts of the pattern were calculated [27]. It has been

observed that the percentage crystallinity of the composites increases with filler fraction. It reveals the crystalline nature of Pd(acac).

However, it decreases after irradiation due to breakage of the bonds and emission of volatile gases, which may form the disordered state in the composite structure. It is also corroborated with FTIR spectra. The values of average crystallite size and % crystallinity of the pristine and irradiated samples are listed in Table 3.1.

**Table 3.1: Average crystallite size and % crystallinity of the composites by XRD analysis**

Sample	Average crystalline size (nm)			% Crystallinity		
	Pristine	$5 \times 10^{12}$ ions/cm <sup>2</sup>	$1 \times 10^{13}$ ions/cm <sup>2</sup>	Pristine	$5 \times 10^{12}$ ions/cm <sup>2</sup>	$1 \times 10^{13}$ ions/cm <sup>2</sup>
PMMA+10% Pd(acac)	6.6	5.7	3.8	10.2	10.0	10.0
PMMA+20% Pd(acac)	15.6	11.4	11.3	15.6	13.4	11.2
PMMA+30% Pd(acac)	22.7	18.1	16.0	17.3	14.3	13.2
PMMA+40% Pd(acac)	23.4	23	22.2	38.8	37.7	25.5

### 3.2.3 FTIR spectroscopy

Fig. 3.11(a,b) shows FTIR spectra of pristine and irradiated ( $5 \times 10^{12}$  ions/cm<sup>2</sup>) samples. The presence of different functional groups in pure PMMA is identified as follow: (A) the bond corresponds to -OH free stretching vibration has been obtained at  $3610 \text{ cm}^{-1}$ , (B) the broad band between  $2835\text{-}2995 \text{ cm}^{-1}$  assigned for -CH<sub>2</sub> group [17], (C) C=C stretching vibration is obtained at  $2050 \text{ cm}^{-1}$ . (D) nonconjugated C=O ester stretching band in pendant group of PMMA (-COOCH<sub>3</sub>) observed at  $1700 \text{ cm}^{-1}$ . (E) The band at  $966 \text{ cm}^{-1}$  corresponds to CH=CH (trans) [28].

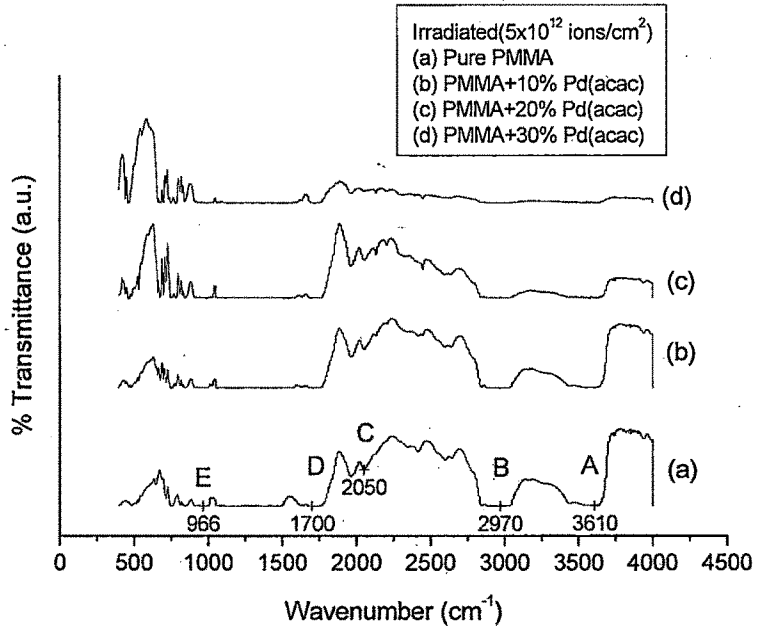
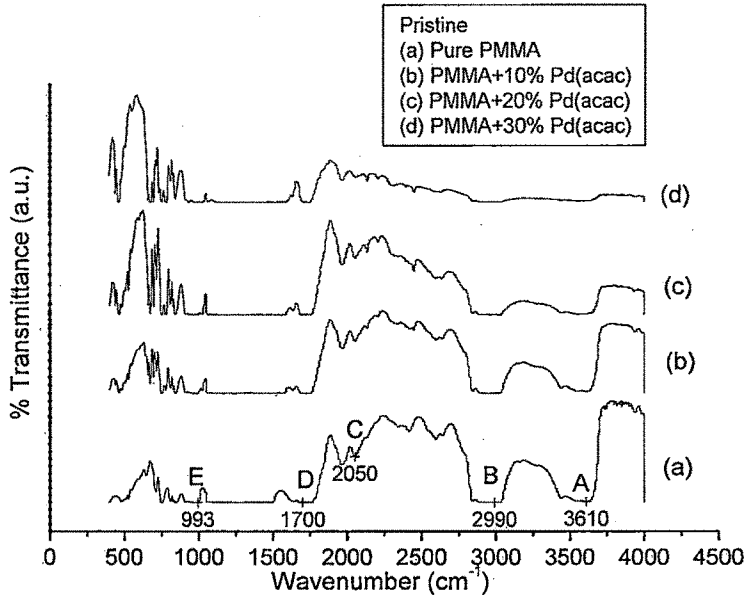


Fig. 3.11 FTIR spectra of (a) Pristine and (b) Irradiated ( $5 \times 10^{12}$  ions/ $\text{cm}^2$ ) films

The reduction in peak intensities after irradiation attributes the breakage of chemical bonds and formation of free radicals, unsaturation etc. due to the deposition of energy by ion beam. The absorption peaks at higher wavenumber decrease sharply as filler concentration increases. It might be due to the formation of new bond of organometallic compound with polymeric chains by breaking traditional polymeric bond and this may be the reason for the formation of new peaks at lower wave number region ( $\sim 500\text{-}800\text{ cm}^{-1}$ ). The overall reduction in intensity of the typical bands after irradiation signifies the chain scissioning phenomenon of the polymeric materials and conversion of polymeric structure into hydrogen depleted carbon network due to the emission of hydrogen and/or other volatile gases [24].

### 3.2.4 Atomic force microscopy

Surface morphology of pristine and irradiated composites was studied by using atomic force microscopy in tapping mode with silicon nitride ( $\text{Si}_3\text{N}_4$ ) tip. Surface morphology of pristine and irradiated (at a fluence of  $5 \times 10^{12}$  ions/ $\text{cm}^2$ ) samples are shown in Fig 3.12 (a-d) in  $2 \times 2\ \mu\text{m}^2$  area.

Average surface roughness was observed to decrease from 7.6 nm to 2.4 nm for PMMA+10% Pd(acac) and 11.4 nm to 9.8 nm for PMMA+30% Pd(acac) after irradiation. It indicates that the proton beam irradiation makes the polymeric surface relatively smoother. This decrease in roughness is attributed to defect-enhanced surface diffusion [19-21]. However, the increase in roughness with concentration of filler is ascribed to increase in density and size of metal particle on the surface of PMMA films [22, 23].

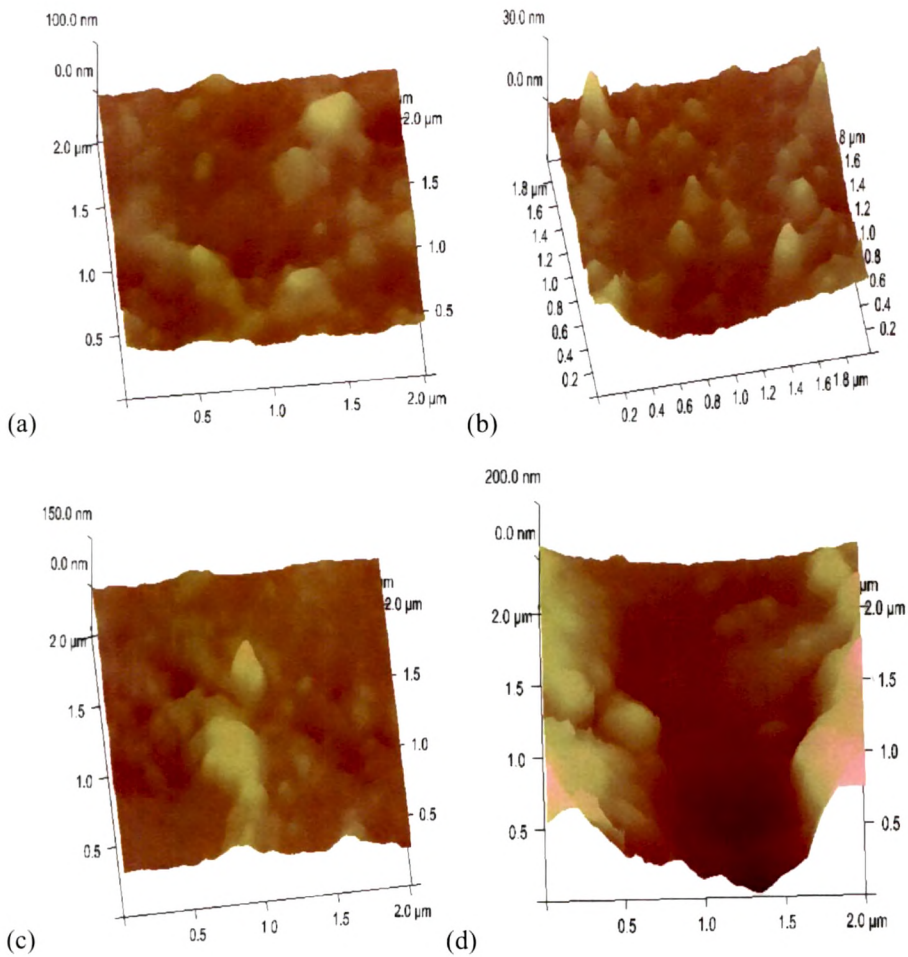


**Fig. 3.12 AFM images of (a) PMMA+10%Pd(acac)-Pristine (b) PMMA+10%Pd(acac)-Irradiated (c) PMMA+30%Pd(acac)-Pristine (d) PMMA+30%Pd(acac)-Irradiated**

### 3.2.5 Scanning electron microscopy

Fig.3.13 (a,c,e) represents pristine and Fig 3.13 (b,d,f) represents irradiated images of pure PMMA, PMMA+10% Pd(acac) and PMMA+40%Pd(acac) respectively. Surface morphology of composites shows appreciable change after proton beam irradiation.

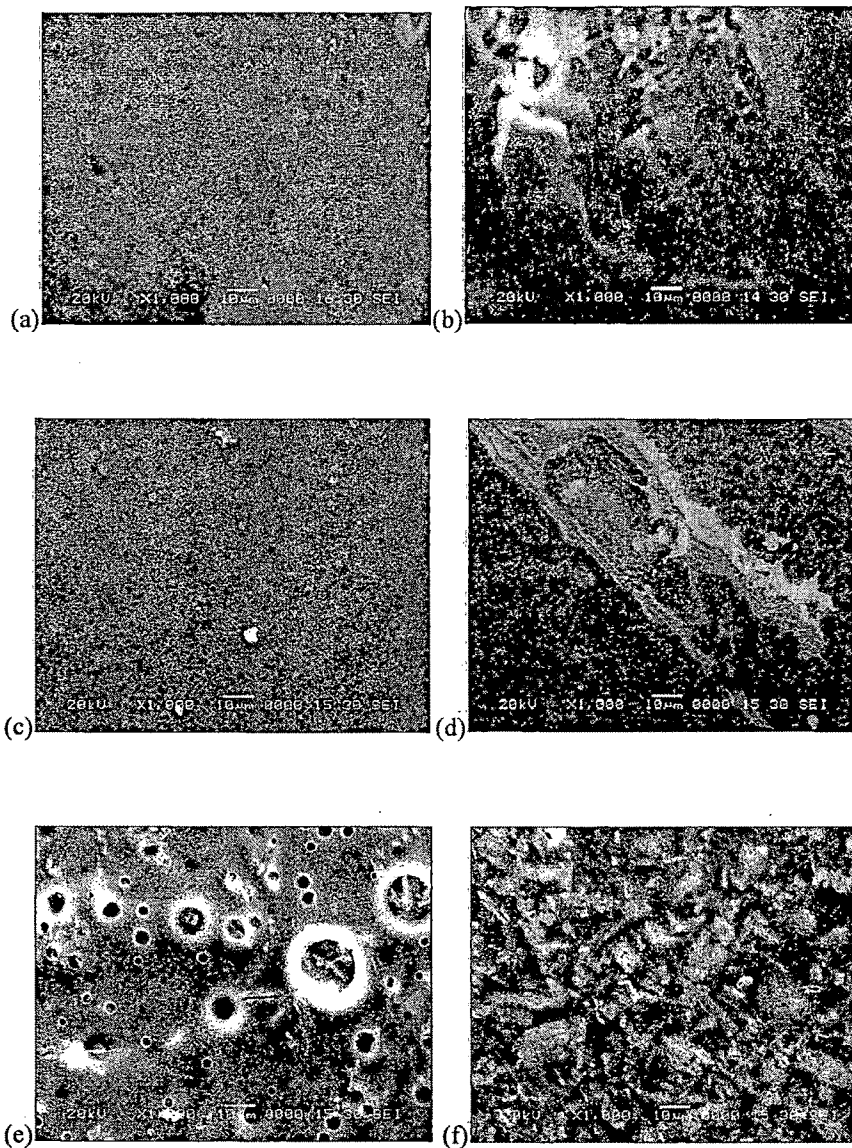


Fig 3.13 SEM images of (a) Pure PMMA-pristine (b) Pure PMMA-irradiated (c) PMMA+10%Pd (acac)-pristine (d) PMMA+10%Pd (acac)-irradiated (e) PMMA+30%Pd (acac)-pristine and (f) PMMA+30%Pd (acac)-irradiated films.

### 3.2.6 Differential scanning calorimetry (DSC)

Fig. 3.18 shows DSC thermograms of pristine PMMA, pristine and irradiated PMMA+40%Pd(acac) samples. The result reveals that the glass transition temperature ( $T_g$ ) increases for the composite than that of the pure polymer but decreases after irradiation.

Glass transition temperature is characteristic of a material and represents the transition from amorphous glassy state to rubbery state. The increase in  $T_g$  of composites may be due to interactions of Pd(acac) and PMMA in more ordered state [29]. After irradiation  $T_g$  decreases, which reveals the amorphization of the composite which is also corroborated with XRD results.

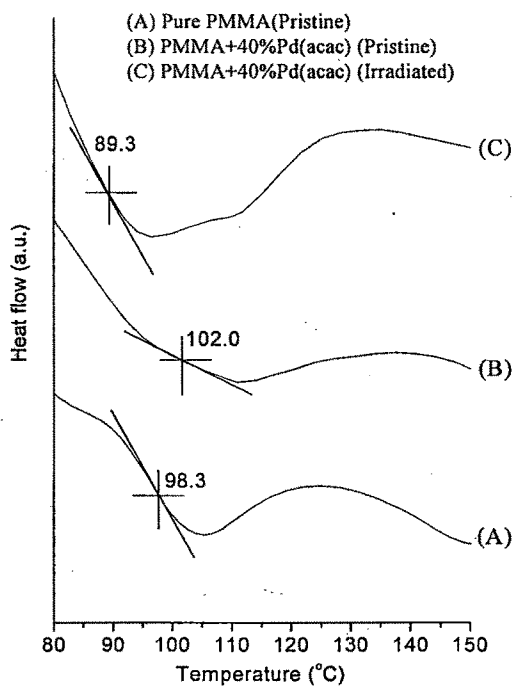


Fig. 3.18 DSC patterns for pure PMMA (pristine) and pristine and irradiated PMMA+40% Pd (acac) films

### 3.2.7 Conclusions

Proton irradiation has significantly enhanced electrical and mechanical properties of polymer composites. This is attributed to the fact that the radiation exposure on the polymeric composites converts the polymeric structure into hydrogen depleted carbon network and promotes good bonding between metal and polymer. This makes the composite more conductive and harder. XRD results depict that crystallite size and degree of crystallinity decreased with ion fluence, however, it increases with increasing filler concentration. The chain scission by irradiation at higher fluence seems to be the dominant process as studied by using FTIR spectroscopy. The surface morphology as studied from SEM images shows partial agglomeration on the composite surfaces after irradiation. AFM results show a decrease in average surface roughness after irradiation. It might be attributed to defect enhanced surface diffusion. DSC analysis shows that  $T_g$  decreases with irradiation due to amorphization of material which is also corroborated with XRD analysis. In general, proton beam irradiation enhances dielectric property of the material nevertheless the structural property degrades up to certain extent.

### 3.3 Effect of proton beam on PMMA+Ni composites

#### 3.3.1 AC electrical properties

##### (i) AC electrical Conductivity

Fig. 3.15(a,b) shows the frequency dependent electrical conductivity (calculated using eq. 2.3.13 in Chapter-2) of pristine and irradiated composites and Fig. 3.15(c) shows the dependence of conductivity on filler concentration at a frequency of 1 MHz.

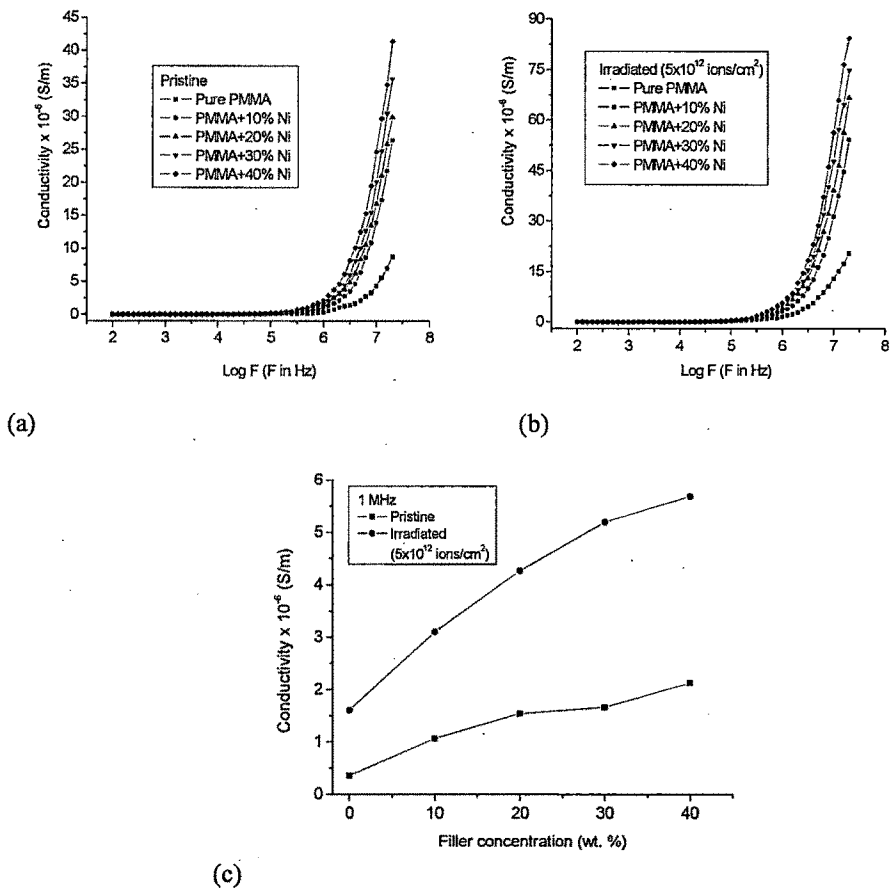


Fig. 3.15 Conductivity vs. log frequency for (a) Pristine and (b) Irradiated composite films, (c) Conductivity vs. filler concentration at 1 MHz.

The result states that the conductivity significantly changes with metal concentration and also with the ion fluence. Further, almost all samples show similar results up to 10 kHz, typical for hopping conduction, means there is no much change in the conductivity with frequency in this range. The total conductivity of the composite depends on the microscopic and macroscopic conductivities. The microscopic conductivity depends upon the doping level, chain length etc. and the macroscopic conductivity depends upon the orderness and molecular orientations in the material [15]. The orderness increases with increasing metal concentration in the composite which is approved by XRD analysis and it is also responsible for increasing the conductivity. The increase in conductivity is related to a possible increase in the number of conduction paths created between the filler particles aggregates in the composite as a consequence electrical path is built in the polymer matrix in addition to a decrease in the width of potential barriers within the bulk regions of high conductivity. Therefore, more charge carriers may be able to 'hop' by tunnelling; resulting in the increase in the bulk conductivity and it also increases with increasing filler concentration. Conductivity is further observed to increase after irradiation. Irradiation is expected to promote the metal to polymer bonding and convert polymeric structure into hydrogen depleted carbon network. It is this carbon network that is believed to make the polymer more conductive [11].

*(ii) Dielectric properties*

Fig. 3.16(a, b) and Fig. 3.17(a, b) show the dependence of dielectric constant and loss tangent respectively on the frequency of the applied field, filler concentration and irradiation fluence. Fig. 3.16(c) shows variation in dielectric constant with filler

concentration at fixed frequency (i.e. 1 MHz) for pristine and irradiated samples. It was calculated using equation 2.3.15 (Chapter-2).

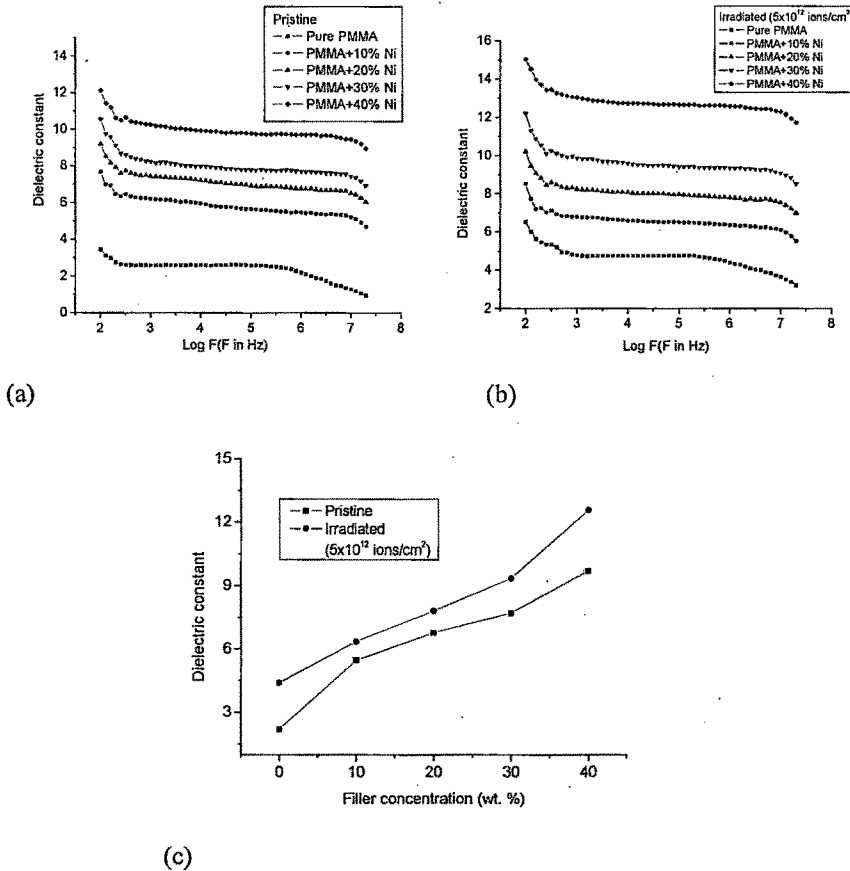


Fig. 3.16 Dielectric constant vs. log frequency for (a) Pristine and (b) Irradiated composites, (c) Dielectric constant vs. filler concentration at 1 MHz

The dielectric permittivity as a function of frequency (1 MHz) reflects the important effect of the filler concentration on the sample properties. The increase in dielectric permittivity with metal concentration is attributed to the increase in the volume fraction of the charges (electric dipoles) at the interfaces between polymer and metal particles. Ions under low frequency electric field can hop readily out of sites with low free energy barriers but tend to 'pile up' at sites with high free

energy barriers. This leads to a net polarization of the dipoles and large value of dielectric permittivity. At higher frequencies, the polarization due to charge 'pile up' disappears and so dielectric constant decreases [30]. Thus the dielectric constant remains almost constant for wide frequency range. Similar results have been also obtained previously [31, 32].

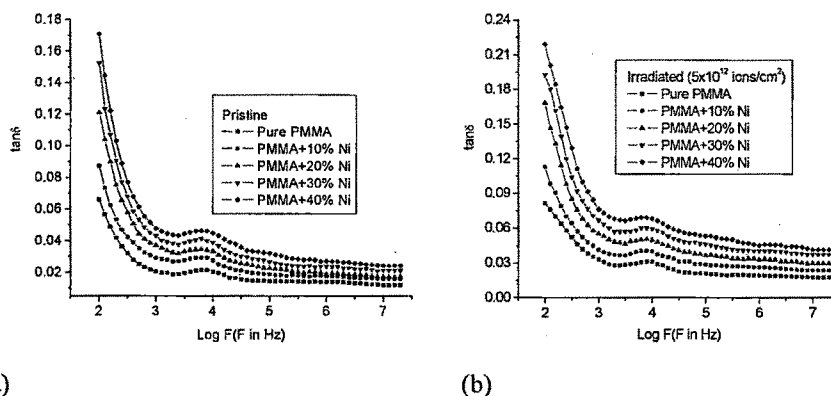


Fig. 3.17 Dielectric loss ( $\tan\delta$ ) vs. log frequency for (a) Pristine and (b) Irradiated composites

In addition, the dependence of dielectric constant on frequency can be explained according to Jonscher's equation described as follows:

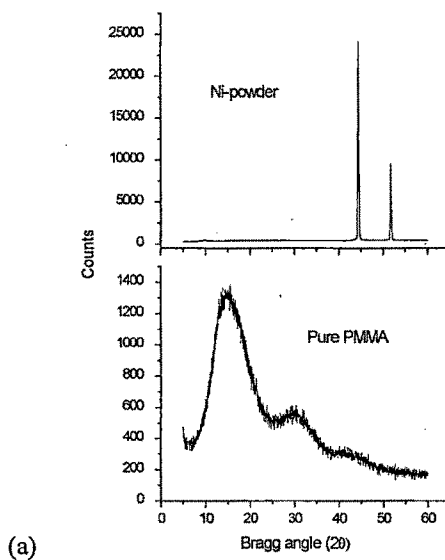
$$\text{i.e. } \epsilon \propto f^{n-1}$$

where  $\epsilon$  is dielectric constant of the sample and  $0 < n < 1$  [15]. Due to the dispersion of metal particles, the quantity of the accumulated charges will increase because of the polarization at polymer/metal interfaces. The polarization makes an additional contribution to the charge quantity. From this point of view, the dielectric constant of the composites will be higher than the pure polymer. High dielectric constant and dielectric loss at higher concentration of nickel in the polymer is attributed to the increase in crystallinity as revealed from XRD analysis. As a result the

orderliness increases the interfacial interactions between the polymer and metal particles and leads to maximum space charge polarization [33]. The observed nature of fluence dependent dielectric constant and dielectric loss can be explained by the prevailing influence of the enhanced free carriers due to irradiation [34].

### 3.3.2 X-ray diffraction

X-ray diffraction spectrum in Fig. 3.18(a) shows the amorphous nature of PMMA and the crystalline behaviour of Ni powder. The average particle size of the Ni powder was obtained 39.8 nm. From Fig. 3.18(b) and (c) the most prominent peaks are obtained at  $2\theta \sim 51.9$  and  $44.6$  in all the cases. The appearance of sharp peak in composites indicates some degree of crystallinity, although the decrease in intensity of the diffraction peak and slightly broadening of the peak after irradiation gives evidence of decrease in crystallinity. However no significant change in the peak position reveals that lattice parameters do not change significantly.



(a)

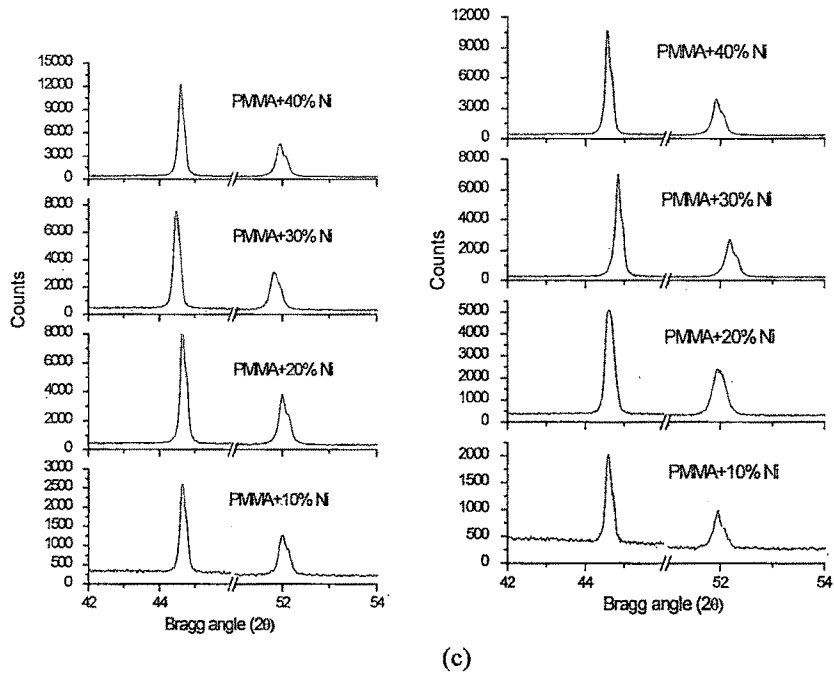


Fig. 3.18 XRD spectrum of (a) Pure PMMA and filler (Ni -powder), (b) Pristine and (c) Irradiated ( $5 \times 10^{12}$  ions/cm<sup>2</sup>) composites

The crystallite size has been calculated before and after irradiation using Scherrer's formula [25]

$$D = \frac{K\lambda}{l \cos \theta}$$

where K is constant approximately equal to unity and related to the crystalline shape,  $l$  is FWHM of the diffraction peak, D is crystalline size and  $\theta$  is the angle between the atomic plane and both the incident and reflected beams.

Percentage crystallinity of the composites was determined by area ratio method. In this method the areas of amorphous and crystalline parts of the pattern were calculated [27]. The average crystallite size and % crystallinity of the pristine and irradiated samples are listed in Table 3.2.

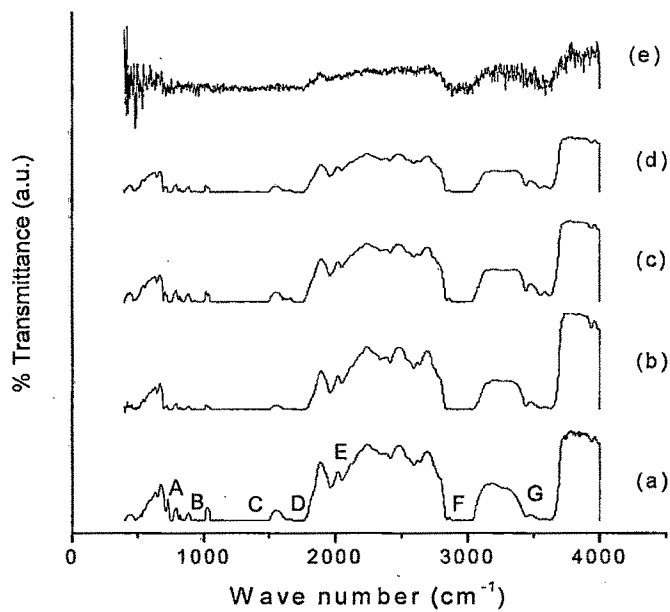
Table 3.2: % Crystallinity and crystalline size of the filler

Filler concentration (wt.%)	Average crystalline size (nm)		% Crystallinity	
	Pristine	$5 \times 10^{12}$ ions/cm <sup>2</sup>	Pristine	$5 \times 10^{12}$ ions/cm <sup>2</sup>
10	34.7	27.8	12.4	6.7
20	36.8	28.3	19.5	18.3
30	37.2	34.9	23.7	16.1
40	38.2	36.6	25.4	25

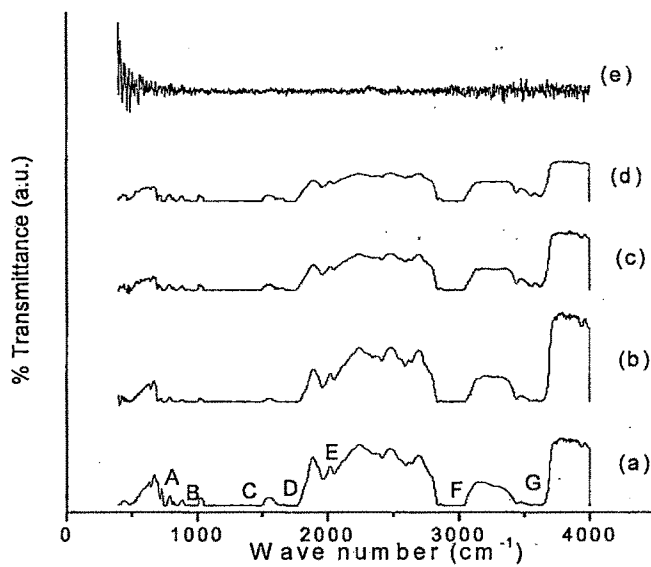
Irradiation induces large amount of energy deposition in the material which leads to decrease in crystallite size which may be attributed to splitting of crystalline grains. The chain scissioning due to irradiation, which is also corroborated with FTIR analysis, assumed to be responsible for the reduction in crystallinity of the composite.

### 3.3.3 FTIR Spectroscopy

FTIR spectra of pristine and irradiated composite films are shown in Fig. 3.19 (i, ii) respectively. The absorption bands are obtained from the pristine spectrum which are identified as follows: (A) 750- 810 cm<sup>-1</sup>: CH<sub>2</sub> rocking vibration, (B) 700-1500 cm<sup>-1</sup>: C=O stretching vibration, (C) 1350-1450 cm<sup>-1</sup>: C-H bending vibration, (D) 1700 cm<sup>-1</sup>: nonconjugated C=O ester stretching band in pendant group of PMMA (-COOCH<sub>3</sub>) (E) 2010 cm<sup>-1</sup>: C=C stretching vibration, (F) 2835-2995 cm<sup>-1</sup>: -CH<sub>2</sub> group and (G) 3610 cm<sup>-1</sup>: -OH free stretching vibration [24]. FTIR spectra show the interaction between macromolecule and filler particles. Small shift and alteration in the peak position is observed due to changes in the nearest surrounding of functional groups because of the presence of metal particles.



(i)



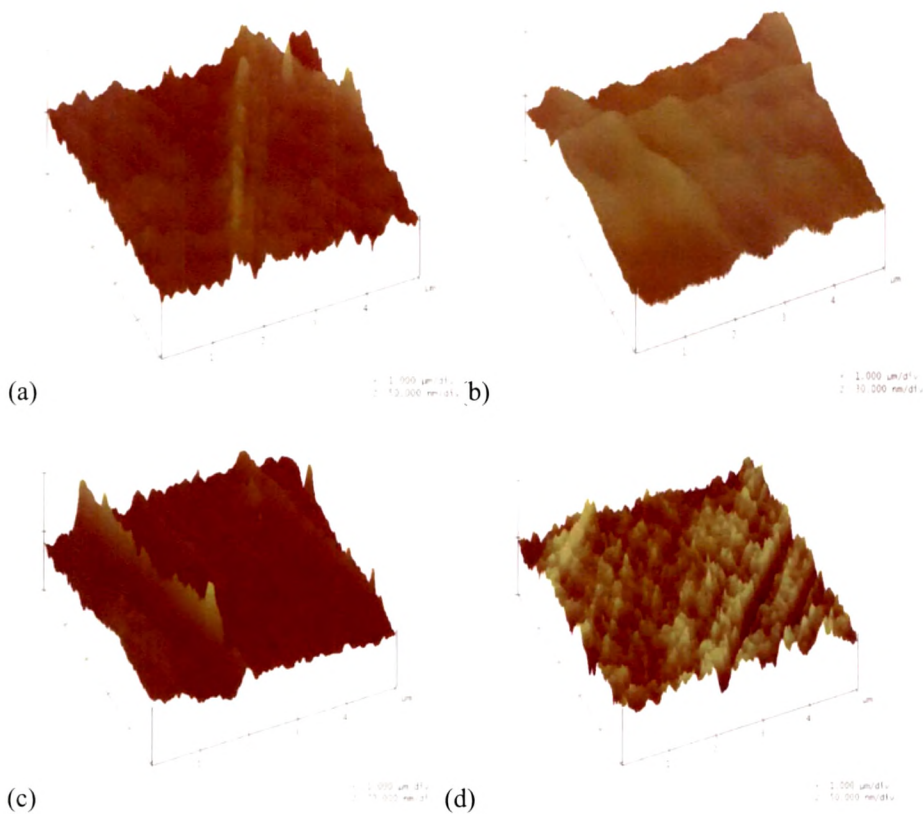
(ii)

Fig. 3.19 FTIR Spectra of (i) Pristine and (ii) Irradiated films of (a) Pure PMMA, (b) PMMA+10%Ni, (c) PMMA+20%Ni, (d) PMMA+30%Ni and (e) PMMA+40%Ni

The peak corresponding to -OH stretching vibration for pristine PMMA was observed at  $3610\text{ cm}^{-1}$  and it shifted to  $3620\text{ cm}^{-1}$  for 30% Ni doped polymer. The reduction in peak intensities after irradiation is attributed to the breakage of few chemical bonds and formation of free radicals, unsaturation, etc. due to emission of hydrogen and/or other volatile gases. However, metal and polymer are extremely different materials, the interaction between metal and polymer is generally very weak. Cohesive energy of polymer is typically two orders of magnitude lower than the cohesive energy of metals. It is observed that the hardness of the composite increases after doping metal particle which indicates the cross linking phenomenon [21].

### **3.3.4 Atomic Force Microscopy**

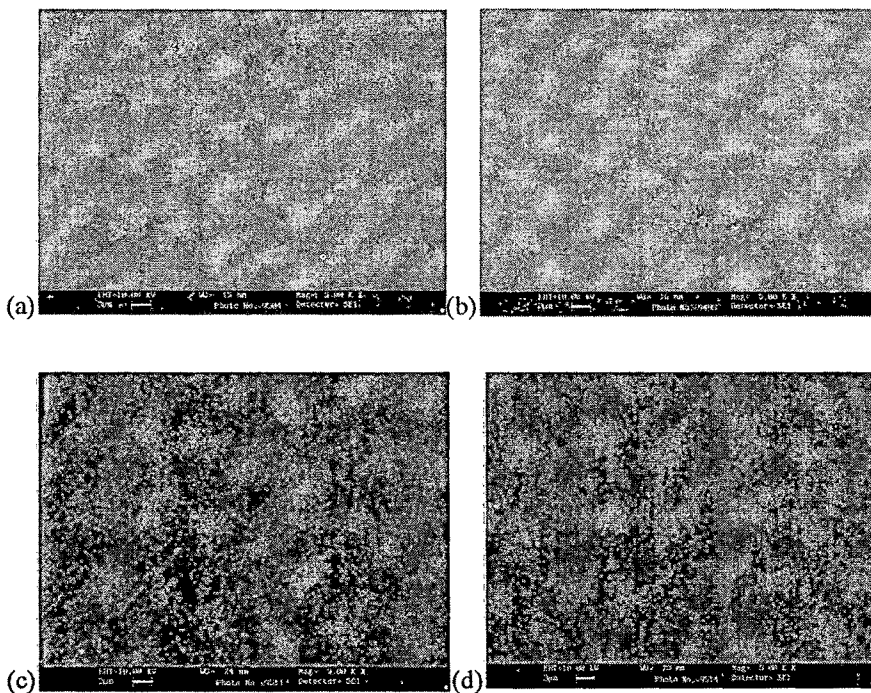
Surface morphology of pristine and irradiated composites was studied using atomic force microscopy in tapping mode. The images of the  $5 \times 5\ \mu\text{m}^2$  surface area of pristine and irradiated (at a fluence of  $5 \times 10^{12}\text{ ions/cm}^2$ ) samples are shown in Fig. 3.20(a-f). The average surface roughness value decreases from 6.2 and 9.3 nm to 4.7 and 5.0 nm respectively for 20 and 30% nickel dispersed PMMA composites after irradiation. The relative smoothness is envisaged because of defect enhanced surface diffusion [19]. However the increase in roughness with filler concentration is attributed to increase in density and size of metal particle on the surface of PMMA films [22, 23].



**Fig. 3.20 AFM images of (a) Pristine PMMA+20% Ni (b) Irradiated PMMA+20% Ni (c) Pristine PMMA+30% Ni (d) Irradiated PMMA+30% Ni films**

### **3.3.5 Scanning electron microscopy**

SEM images were taken for pristine and irradiated samples of 10% and 20% Ni dispersed PMMA composites at 5 kX magnification. No significant change in surface topography was observed after irradiation. Fig. 3.21(a-d) shows SEM images of pristine and irradiated composites.



3.21 SEM images of (a) PMMA+10% Ni (pristine) (b) PMMA+10%Ni (irradiated) (c) PMMA+20% Ni(Pristine) (d) PMMA+20% Ni(Irradiated) films

### 3.3.6 Conclusions

Proton beam has significantly enhanced the electrical properties of the composites. This may be attributed to metal to polymer bonding and conversion of polymeric structure in to hydrogen depleted carbon network. Structural properties have observed to change due to irradiation. The crystallite size and % crystallinity decreased after irradiation. The decrease in % crystallinity reveals the formation of disorderness in the sample due to chain scissioning after irradiation. It is also corroborated with FTIR spectroscopy. The average surface roughness of the samples decreases upon irradiation however, no significant change is observed from SEM images.

### 3.4 Effect of proton beam on PMMA+Ni-DMG composites

#### 3.4.1 AC electrical properties

##### (i) AC electrical Conductivity

Figure 3.22 shows the variation of conductivity with log frequency, calculated using equation 2.3.13 as discussed in Chapter-2. It is observed that conductivity increases with increasing concentration of dispersed Ni-DMG compound (Fig. 3.22(a)) as well as after irradiation (Fig. 3.22(b)).

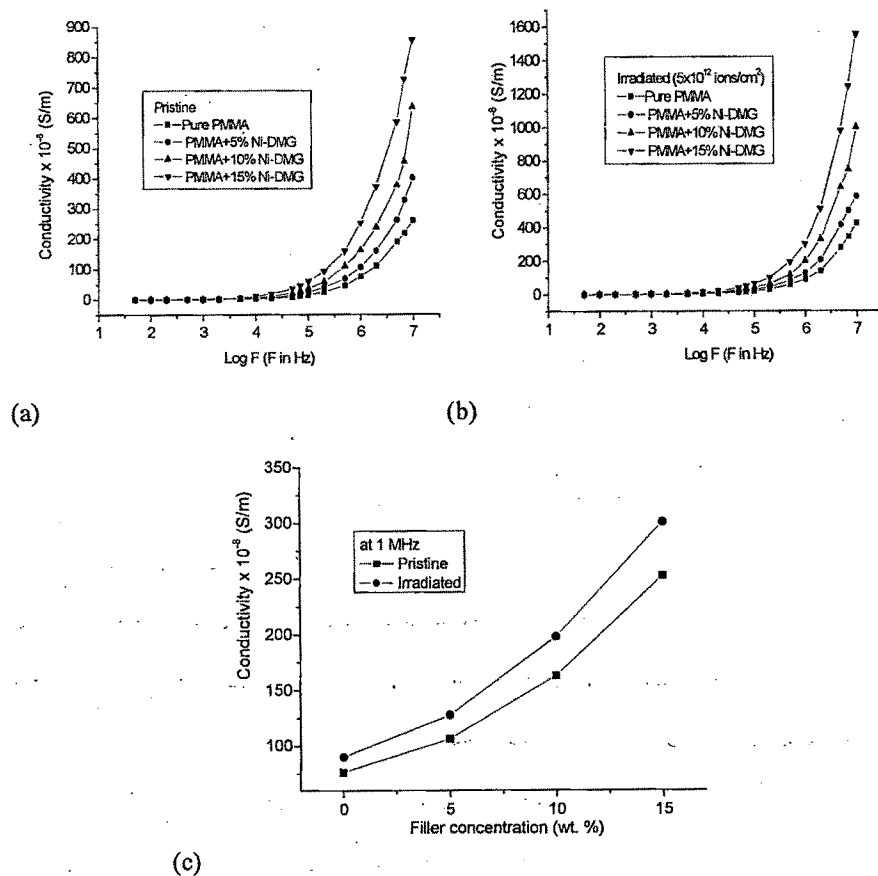


Fig. 3.22 Conductivity vs. log frequency for (a) Pristine and (b) Irradiated composites (c) Conductivity vs. filler concentration at 1 MHz

The increase in conductivity with increasing concentrations of organometallic compound may be attributed to the conductive phase formed by dispersed organometallic compound in polymer matrix. It is known that electrical conductivity of such composites depends on the type and concentration of the dispersed compound. Fig. 3.22(c) shows variation in conductivity with filler concentrations. The conductivity of dispersed films increases with increasing the concentration of Ni-DMG compound in polymer matrix. The conductivity is also observed to increase after the irradiation. Irradiation is expected to promote the metal to polymer adhesion and convert the polymeric structure into a hydrogen depleted carbon network. It is this carbon network that is believed to make the polymer more conductive [11, 35].

*(ii) Dielectric properties*

Fig. 3.23 shows the variation in dielectric permittivity with log frequency calculated using equation 2.3.15 (Chapter-2). It is observed that dielectric permittivity remains almost constant up to 100 kHz, because the motion of charge carriers is almost constant at these frequencies. Beyond this frequency, the dielectric constant decreases. As the frequency increases, the charge carriers migrate through the dielectric and get trapped against a defect sites and they induced an opposite charge in its vicinity, as a result, motion of charge carriers is slowed down and the value of dielectric constant decreases. The decrease in dielectric constant at higher frequency can be explained by Jonscher's power law i.e.  $\epsilon \propto f^{-n}$  where  $0 < n < 1$  [15]. The value of  $n$  increases on irradiation from 0.26 to 0.56 for pure PMMA. Similar results are also observed for dispersed PMMA. This may be due to the dominance of metal to polymer bonding due to irradiation, which reduces the dipole polarization and as a result,  $\text{slop}(n)$  increases.

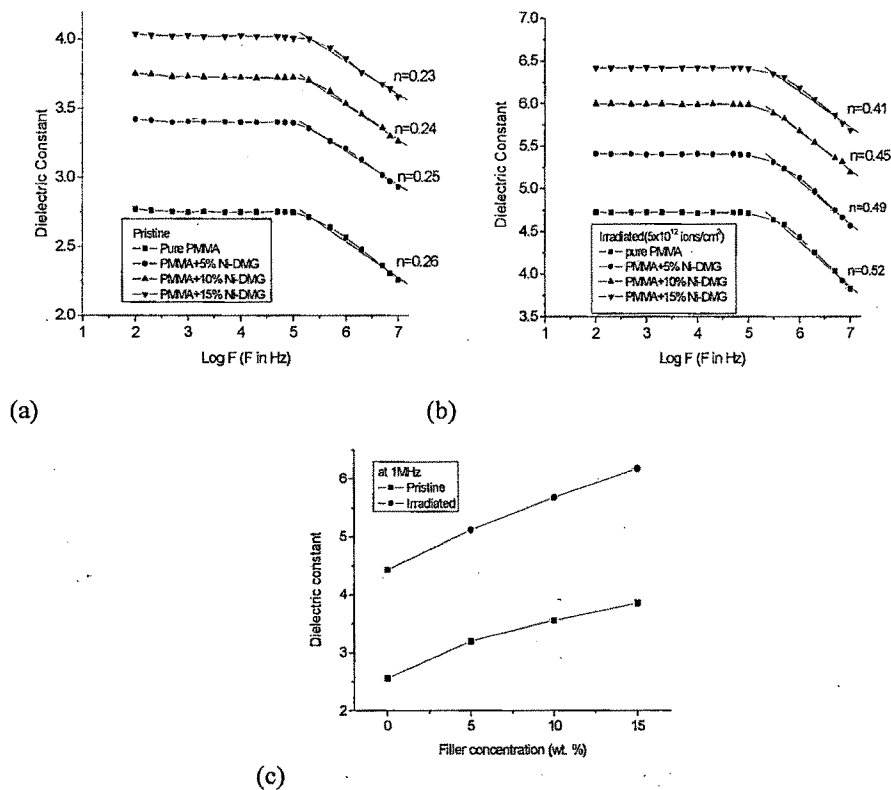


Fig. 3.23 Dielectric constant vs. log frequency for (a) Pristine and (b) Irradiated composites, (c) Dielectric constant vs. filler concentration at 1 MHz

According to Dissado and Hill [36] theory at high frequency, intra-cluster motions are dominant. In intra-cluster motions, the relaxation of a dipole will produce a 'chain' response in its neighboring dipoles and the reaction of the neighboring dipoles will, in turn, affect the first dipole, so the overall effect will be seen as a single cluster dipole moment relaxation [15]. This reduces the dielectric constant at these frequencies.

It is observed that the dielectric constant increases on increasing the concentration of Ni-DMG. Fig. 3.23 (c) shows variation in dielectric constant with filler concentration. Due to dispersion of organometallic compound, the quantity of accumulated charge will increase because of the polarization of polymer/metal at

interfaces. The polarization makes an additional contribution to the charge quantity. From this point of view, the dielectric constant of the composites will be higher than the pure polymer [14]. The magnitude of the dielectric constant is higher for irradiated samples compared to those of pristine samples. The increase in dielectric constant may be attributed to chain scission, which results in an increase of free radicals, unsaturation etc.

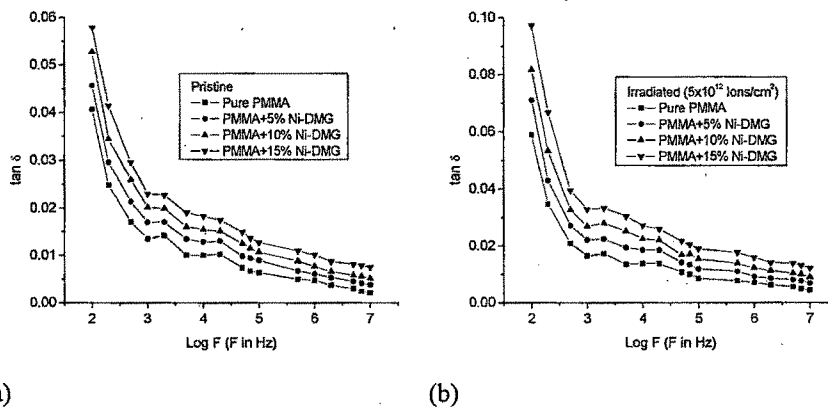


Fig. 3.24 Dielectric loss vs. log frequency for (a) Pristine and (b) Irradiated composites

Figure 3.24 (a, b) shows the behavior of dielectric loss with frequency for pure and dispersed Ni-DMG samples at room temperature. The loss factor ( $\tan\delta$ ) shows strong frequency dependence and decreases exponentially as frequency increases. The positive value of  $\tan\delta$  indicates the dominance of inductive behaviour [12]. It is noticed that dielectric loss increases with increasing the concentration of filler and also with the irradiation fluence. The increase in dielectric loss with increasing filler contents may be attributed to the interfacial polarization mechanism of the heterogeneous system.

### 3.4.2 X-ray Diffraction

Fig. 3.25 (a, b) represents the diffraction pattern of the pristine and irradiated samples for the most prominent peak. The peaks are obtained at  $2\theta = 9.98$  and  $10.61$ .

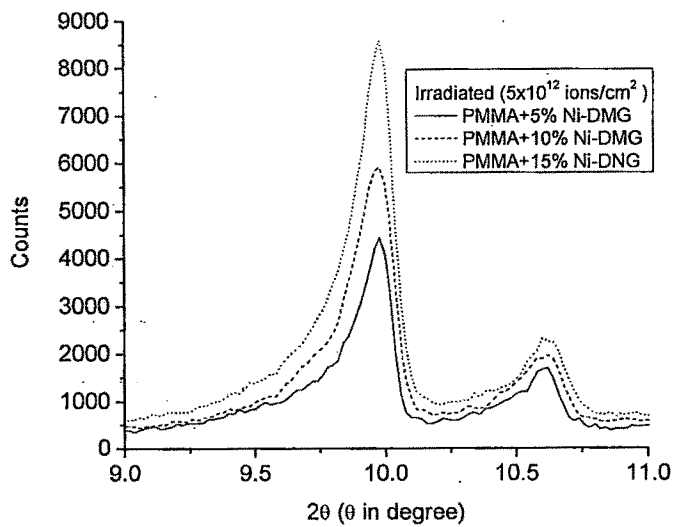
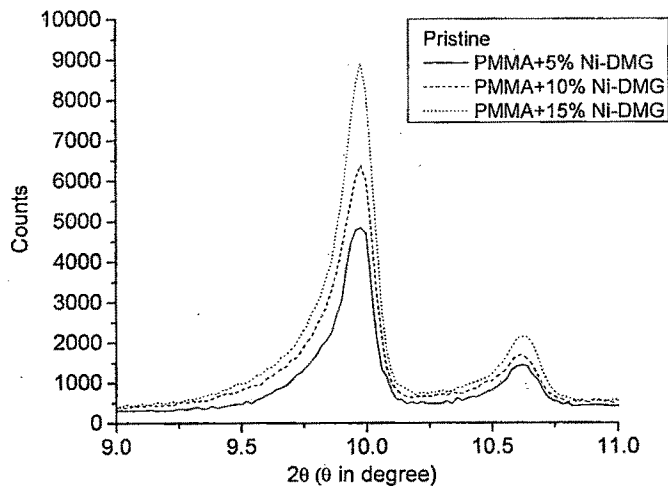


Fig. 3.25 XRD pattern of (a) Pristine and (b) Irradiated samples

The nature of the peak indicates the semi-crystalline nature of the sample. The crystallite size was calculated before and after irradiation using Scherrer's equation [25] as explained in section 2.3.3 of Chapter-2.

$$D = \frac{K\lambda}{l \cos \theta}$$

where K is constant approximately equal to unity and related to the crystalline shape,  $l$  is FWHM of the diffraction peak, D is crystalline size and  $\theta$  is the angle between the atomic plane and both the incident and reflected beams.

The crystallite size obtained using above equation is listed in Table 3.3.

Results show that crystallite size of the filler decreases slightly after irradiation. It is also observed that the intensity of the peak decreases after irradiation, but no significant change in the peak position has been observed. This reveals that the lattice parameters do not change significantly but crystallinity of the sample decreases after irradiation [37].

**Table 3.3: Crystallite size of the pristine and irradiated samples by XRD**

Sample	Crystallite size(nm)	
	Pristine	Irradiated( $5 \times 10^{12}$ ions/cm <sup>2</sup> )
PMMA+5%Ni-DMG	45.6	44.6
PMMA+10% Ni-DMG	47.7	45.0
PMMA+15%Ni-DMG	48.5	45.7

### 3.4.3 Atomic Force Microscopy (AFM)

Surface morphology of the pristine and irradiated metallized polymeric samples has been studied using atomic force microscopy. The images of  $2 \times 2 \mu\text{m}^2$  area were

recorded in tapping mode as shown in Fig. 3.26 (a-f). Each AFM image was analyzed in terms of surface average roughness ( $R_a$ ). The data shows that the surface average roughness (rms) increases with metal compound (Ni-DMG) concentrations but it decreases after irradiation.

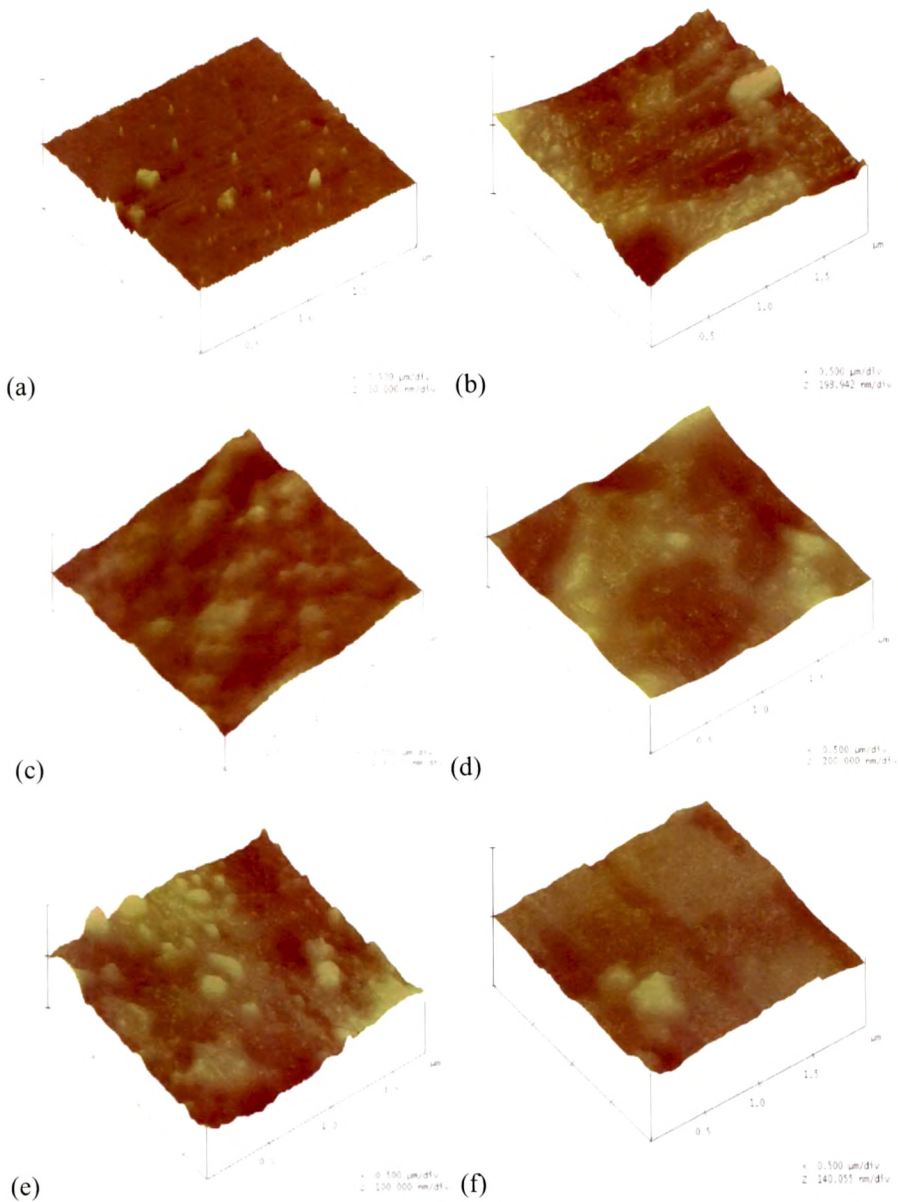


**Fig. 3.26 AFM image of (a) PMMA+5%Ni-DMG(pristine), (b) PMMA+5%Ni-DMG(irradiated), (c)PMMA+10%Ni-DMG(pristine), (d) PMMA+10%Ni-DMG(irradiated), (e) PMMA+15%Ni-DMG(pristine), (f)PMMA+15%Ni-DMG(irradiated) films**

The average surface roughness obtained are 8.6 nm, 32.4 nm and 36.6 nm for pristine samples with filler concentrations of 5%, 10% and 15% respectively and decreases to 6.5 nm, 10.7 nm and 11.9 nm after irradiating at a fluence of  $5 \times 10^{12}$  ions/cm<sup>2</sup>. The increase in surface roughness ( $R_a$ ) with increase in concentration of metal compound may be due to the increase of density and size of metal particles on the surfaces of the polymeric films [22, 23]. The decrease in surface roughness due to irradiation may be attributed to defect enhanced surface diffusion.

#### **3.4.4 Conclusion**

Dispersion of organometallic compound (Ni-DMG) in PMMA films has enhanced the properties of the pure polymer significantly. The increase in dielectric properties with filler concentration may be attributed to the conductive phase formed by dispersed organometallic compound in polymer matrix. Further enhancement in dielectric properties was observed after proton irradiation. It may be due to the metal to polymer adhesion and conversion of the polymeric structure into a hydrogen depleted carbon network. AFM analysis revealed that the proton irradiation makes the surface of the sample smoother. This relative smoothness is probably due to the sputtering effects and as a consequence surface diffusion. An XRD analysis reveals that the crystallite size decreased after ion beam irradiation.

### 3:5 Summary

Four different composites have been studied using proton beam irradiation. AC electrical, mechanical, structural, thermal and surface properties have been investigated using different characterization techniques.

AC electrical conductivity of all pristine and irradiated composites at 10% filler concentration is shown in Fig. 3.27. The increase in conductivity is related to a possible increase in the number of conduction paths created because of filler particles aggregate in the polymer matrix. Therefore, more charge carriers may be able to 'hop' by tunnelling; resulting in the increase in the bulk conductivity and it also increases with increasing filler concentration. Conductivity is further observed to increase after irradiation in all composites. Irradiation is expected to promote the metal to polymer bonding and convert polymeric structure into hydrogen depleted carbon network. This carbon network is believed to make the polymer more conductive and harder. This is the reason to increase the hardness of irradiated PMMA+Fo films. Fig. 3.27 shows comparison of conductivity of all composites before and after irradiation. For the sake of comparison filler fraction (10 wt.%), fluence of proton beam ( $5 \times 10^{12}$  ions/cm<sup>2</sup>) and frequency (10 MHz) have considered constant. Similar study for dielectric constant of all composites have been done and shown in figure 3.28 at a frequency of 10 MHz.

Dielectric loss was studied for all pristine and irradiated composites and result shows frequency and fluence dependent behavior for all cases. In general, the nature of the curves of electrical response for all samples are same but the magnitude varies with filler material.

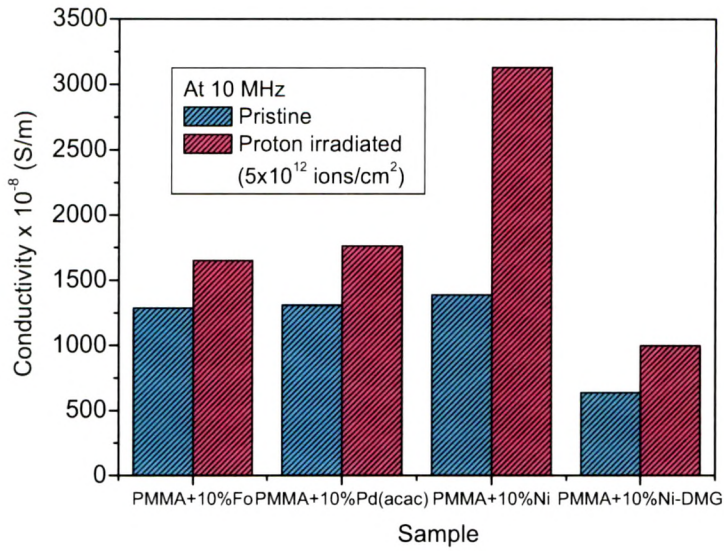


Figure 3.27 Comparison of conductivity of pristine and irradiated ( $5 \times 10^{12}$  ions/cm<sup>2</sup>) composites at 10 MHz frequency

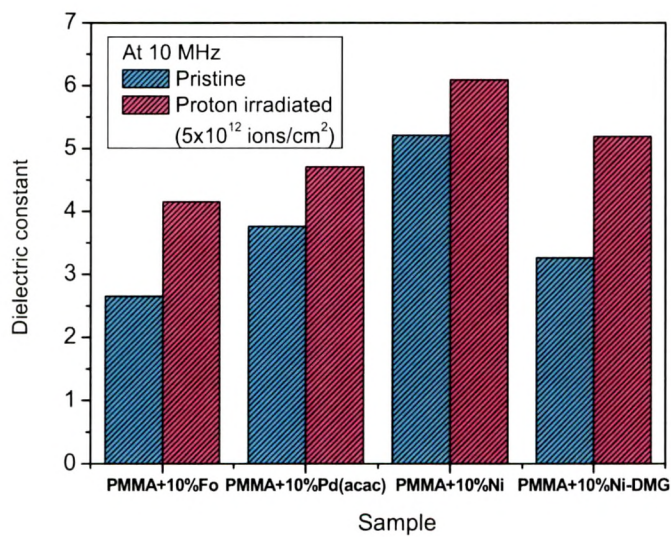


Figure 3.28 Comparison of dielectric constant of pristine and irradiated ( $5 \times 10^{12}$  ions/cm<sup>2</sup>) composites at 10 MHz frequency

XRD of pristine and irradiated samples of PMMA+Pd(acac)/Ni/Ni-DMG have been studied and the results revealed that the crystalline size and % crystallinity of the sample decreases upon irradiation. Irradiation induces large amount of energy deposition in the material, which leads to splitting of crystalline grains and because of that decrease in crystalline size. After irradiation, due to breakage of the polymeric bonds and emission of volatile gases, disorderness increases in composite structure which is responsible for decrease in % crystallinity of composite material.

FTIR images show minute shift and alteration in the peak position of composites due to changes in the nearest surrounding of functional groups because of the presence of filler particles. The reduction in peak intensities after irradiation is attributed to the breakage of few chemical bonds and formation of free radicals, unsaturation, etc. due to emission of hydrogen and/or other volatile gases.

Proton irradiation makes the surface smoother as obtained from AFM analysis. The average surface roughness of all proton irradiated composites decreases than that of the pristine films. The decrease in surface roughness after irradiation might be attributed to defect enhanced surface diffusion.

## References

- [1] Sejal Shah, Anjum Qureshi, N. L. Singh, K. P. Singh, and V. Ganesan, *Soft Materials*, 6(2), (2008) 74-85.
- [2] Sejal Shah, Anjum Qureshi, N.L.Singh, K.P.Singh, D.K.Avasthi, *Radiation measurement*, 43 (2008) S603.
- [3] Sejal Shah, Anjum Qureshi, N.L.Singh, P.K. Kulriya, K.P.Singh, D.K.Avasthi. *Surf. & Coat. Tech.* 203 (2009) 2595.
- [4] Sejal Shah, N.L. Singh, Anjum Qureshi, Dolly Singh, K.P. Singh, V. Shrinet, A. Tripathi, *Nucl. Instrum. Meth. B* 266 (2008) 1768.
- [5] N.L.Singh, Sejal Shah, Anjum Qureshi, K.P.Singh, V. Shrinet, P.K.Kulriya, A. Tripathi *Radiation effects and defects in solids*, 163(2) (2008) 181–189.
- [6] D. Berner, J. P. Travers and P. Rannou *Synth. Met.*, 101 (1999) 836.
- [7] S. R. Krishnan *J. Mater. Sci. Lett.*, 4 (1985) 1445.
- [8] Y. P. Mamunya and Y. V. Muzychenko et al. *Polym. Eng. Sci.*, 42 (2002) 90.
- [9] G. C. Psarras, E. Manolakaki and G. M. Tsangarris. *Composites A.*,33 (2001) 375.
- [10] Z. M. Elimat, *J. Phys. D: Appl. Phys.*, 39 (2006) 2824.
- [11] Y. Q. Wang, M. Curry, E. Tavenner, N. Dobson and R. E. Giedd. *Nucl. Instr. and Meth. B.*,219 (2004) 798.
- [12] N.L.Singh, Nilam Shah, C.F.Desai, K.P.Singh, S.K.Arora. *Radiation Effects & Defects in Solid* 159,475 (2004)
- [13] A. K. Jonscher, *Nature* 267 (1977) 673.
- [14] Zhi-Min Dang, Yi-He Zhang, S.-C. Tjong. *Synthetic Metals* 146 (2004) 79-84.
- [15] A. Pelaiz-Barranco, *Scripta Materialia* 54 (2006) 47.
- [16] W.H. Bowyer and M.G. Bader *J. Mater. Sci.*, 7 (1972) 1315.

- [17] Nilam Shah, Dolly Singh, Sejal Shah, Anjum Qureshi, N.L.Singh, K.P. Singh. *Bulletin of Material Science* **30** (2007) 477.
- [18] E. H. Lee, G. R. Rao, L. K. Mansur, *Mater. Sci. Forum* 248-249 (1997) 135.
- [19] Y. S. Choudhary, S. A. Khan, R. Srivastava, V. R. Satsangi, S. Prakash, U. K. Tiwari, D. K. Avasthi, N. Goswami, S. Dass. *Thin Solid Films* 492 (2005) 332.
- [20] D. C. Aktas, U. Saeed, V. Zaporojtchenko, F. Faupel, R. Gupta, N. Kumar, *Nucl. Instrum. Math B* 217 (2004) 9.
- [21] A.Qureshi, N. L. Singh, A. K. Rakshit, F. Singh, D. K. Avasthi, V. Ganesan. *Surf. And Coat. Tech*, 201 (2007) 8225.
- [22] X. Yan, T. Xu, S. Xu, S. Wang and S. Yang *Nanotechnology*, 15(2004) 1759.
- [23] Sejal Shah, Dolly Singh, Anjum Qureshi, N.L.Singh, K.P.Singh, V. Shrinet. *Ind. J. Pure & Appl. Phy.*, 46 (2008) 439.
- [24] D. Fink, F. Hosoi, H. Omichi, T. Sasuga and L. Amaral. *Rad. Eff. Def. Sol.*, 132 (1994) 313.
- [25] P. Scherrer, *Gott. Nachr*, 2 (1918) 98
- [26] L.V. Azaroff, *Elements of X-ray crystallography* (USA: McGraw Hill Book Co.) (1968) p. 551.
- [27] Serap Kavlak, Hatice Kaplan Can, Ali Guner, Zakir Rzaev, *J. of Applied Polymer Science*, 90 (2003) 1708.
- [28] J. Davenas, X.L. Xu, G. Boiteux, D. Sage, *Nucl. Instr. Meth. B*, 39 (1989) 754.
- [29] T.K. Vishnuvardhan, V.R. Kulkarni, C. Basavaraja, S.C. Raghavendra, *Bull. Mat. Sci*, 29 (2006) 77.
- [30] N.S. Prasad, K.B.R. Varma, *J Non-Cryst Solids* 351 (2005) 1455.
- [31] D.H. Kuo, C.C. Chang et al., *J. Euro. Ceram. Soc.*, 21 (2001) 1171.

- [32] Anjum Qureshi, Ayhan Mergen, Mehmet S. Eroglu, N. L. Singh, Arif Gulluoglu, *J. Macromolecular Sci. A* 45 (2008) 462.
- [33] J. C. Maxwell. *A treatise on electricity and magnetism* (Oxford: Oxford University Press) 1, 1998.
- [34] T. Phukan, D. Kanjilal, T.D. Goswami, H.L. Das, *Nucl. Instr.&Meth. B.* 234 (2005) 520.
- [35] D.K.Avasthi, J.P.Singh, A.Biswas, S.K.Bose. *Nucl. Instr. and Meth. B* 146 (1998) 504.
- [36] L.A. Dissado, R. M. Hill, *Proc. Roy. Soc. London* 390 (1983) 131.
- [37] R. Kumar, U. De, R. Prasad, *Nucl. Instrum and Meth B.* 248 (2006) 279.